Old Dominion University
ODU Digital Commons

Mathematics & Statistics Theses & Dissertations   Mathematics & Statistics

Spring 1995

Thermal Ignition Analysis in the Laminar Boundary Layer Behind a Propagating Shock Front

Mushtaq Ahmed Khan
Old Dominion University

Follow this and additional works at: https://digitalcommons.odu.edu/mathstat_etds

Part of the Mathematics Commons

Thermal Ignition Analysis In The Laminar

Boundary Layer Behind A Propagating Shock Front

by

Mushtaq Ahmad Khan

B.Sc. 1975, Punjab University, Lahore Pakistan
M.S. (Mathematics), 1978, Punjab University, Lahore Pakistan
M.S. (Geophysics), 1982, Quaid-i-Azam University, Islamabad Pakistan

A Dissertation Submitted to the Faculty of
Old Dominion University in Partial Fulfillment of the
Requirements for the Degree of

DOCTOR OF PHILOSOPHY
COMPUTATIONAL AND APPLIED MATHEMATICS

OLD DOMINION UNIVERSITY
April 1995

Approved by:

David Glenn Lasseigne (Director)

Thermal Ignition Analysis in the Laminar Boundary

Layer Behind a Propagating Shock Front

Mushtaq Ahmad Khan

Old Dominion University, 1995

Director: Dr. David Glenn Lasseigne

ABSTRACT

Asymptotic analysis in the limit of large activation energy is performed to investigate the ignition of a reactive gas in the laminar boundary layer behind a propagating shock front. The study is based on a one-step, irreversible Arrhenius reaction of a premixed gas; therefore, the ignition phenomenon is thermally induced. The boundary layer consists of a thin, diffusive, reaction region at the point where the temperature is maximum and diffusive-convective non-reacting regions adjacent to the reacting region. Both adiabatic and isothermal boundary conditions are examined. For the adiabatic wall, the reaction zone is near the insulated boundary. The reaction zone is in the interior for the isothermal wall. The effects of various parameters on the non-dimensional ignition distance and the ignition point are investigated. It is found that the ignition distance decreases almost linearly with the Mach number for both the adiabatic and the isothermal wall cases. In the isothermal wall case with fixed

ii

Mach number, the non-dimensional ignition point decreases linearly with the surface temperature, and the non-dimensional ignition distance has a minimum as the surface temperature varies.

Since the kinetic energy of the supersonic flow is converted into thermal energy through viscous heating in the boundary layer, the dependence of the viscosity on temperature is of particular importance. Sutherland's temperature-viscosity law is used in this research since it is a better approximation and provides a more rapid variation of viscosity with respect to temperature than the linear temperature-viscosity law. Use of the Sutherland's temperature-viscosity law results in coupled momentum and energy equations that are analyzed accordingly. Im, Bechtold and Law [10] did not account for the effects of the shock and used the linear temperature-viscosity law resulting in uncoupled momentum and energy equations. All four cases -Sutherland's law with shock, linear law with shock, Sutherland's law without shock, and linear law without shock- are considered for comparison.

iii

DEDICATION

To my father

iv

ACKNOWLEDGMENTS

I wish to express my sincere gratitude to my advisor, Dr. D. Glenn Lasseigne, for his guidance, patience and encouragement throughout this research work. His friendship and genuine care will not be forgotten soon. I also would like to thank Dr. Fang Q. Hu, Dr. Thomas L. Jackson and Prof. Chester E. Grosch for their helpful comments and suggestions and for serving on my dissertation committee.

I am grateful to all Mathematics faculty and fellow graduate students for their professional contributions and cooperation. I wish to thank Barbara Jeffrey and Gayle Tuckelson for their assistance in many ways.

I express my appreciation to the administration of Norfolk State University for their assistance and cooperation to pursue my studies.

My special thanks to my parents, brothers and sisters for their help and prayers. Special gratitude is also due to my father-in-law, Prof. M. Hanif Hafiz, for his help and being with us at happy and difficult times.

Above all, I sincerely thank my wife, Saeeda, for her support and understanding. Also sincere thanks to my children, Asif, Saima and Aneela, for their patience during many evenings and weekends spent without me.

v

Contents

viii

List of Figures

ix

xi

Chapter 1

INTRODUCTION

Jackson and Kapila [12] and Clark and Cant [6] have shown that an explosive event occurs in a reactive gas between an instantaneously started piston and the strong shock generated by the piston. The ignition stimulus is the relatively large temperature rise behind a shock traveling at Mach number greater than one (relative to the sound speed in the cold gas). The explosion time for the gas in the expanding region between the shock front and an insulated piston is slightly longer than a constant-volume, spatially-homogeneous explosion occurring in the same gas with initial temperature equal to the temperature behind the shock. The induction period is longer in the dynamic situation because a portion of the thermal energy produced by the reaction is converted to kinetic energy resulting in an acceleration of the shock front.

The present analysis is motivated by asking the following question: If the shock front is assumed to propagate parallel to a flat wall, will the increased temperature

1

due to viscous heating ignite the gas so that the ignition event occurs in the thin, viscous boundary layer near the wall and not at the insulated piston?

In an attempt to answer the above question, the following model is analyzed: A planar shock moves through a gas capable of undergoing an exothermic, chemical reaction of the Arrhenius type. The temperature of the gas ahead of the shock front is so low that the gas is considered inert. The shock front moves parallel to a flat wall, and behind the shock front, a boundary layer of the type discussed by Schlichting, H. [16], develops. The effects of heat produced by the chemical reactions initiated by the elevated temperature within the boundary layer are examined. This analysis considers only the ignition of the gas in the boundary layer. This event is short when compared to the spatially-homogeneous explosion time. The study of this model problem does not directly answer the motivating question but provides helpful insight into the initiation of chemical reactions in the boundary layer behind the shock.

The instantaneous acceleration of a piston into a quiescent gas initiates a shock front that travels into the quiescent gas and perpendicular to a flat wall. It is well known that if the shock is freely propagating into an inert gas (i.e., no wall and no reaction), a solution to the one-dimensional equations for gas dynamics relates the speed of the shock to the piston speed (the Rankine-Hugoniot relations), assuming that both the gas between the piston and the shock are moving with uniform speed. If a wall is present, the gas velocity must vanish at the wall; therefore, a boundary

2

layer develops behind the shock and ahead of the piston where the velocity changes from its free-stream value to zero. If the Reynolds number is large, the boundary layer is thin.

The initiation of the chemical reaction immediately behind the shock is considered. For the analysis of chemical processes within the boundary layer to be valid, the distance between the shock front and the piston must be much larger than the boundary-layer thickness and much smaller than the explosion distance. In this time period, the temperature, density, pressure, and velocity of the gas are considered to be constant in the outer, free-stream region; also, the interaction of the boundary layer and the piston is neglected. In essence, the following analysis describes a "steady state" that develops immediately behind the shock.

Since chemically-reacting, boundary layer flows are mostly nonsimilar, the theoretical studies on ignition in subsonic, laminar, boundary-layer flows concerning the issue of nonsimilarity have shown that the ignition distance basically scales linearly with the freestream velocity. These studies include Marble and Adamson [15], Cheng and Kovitz [4] and [5], Dooley [7], Sharma and Sirignano [17], and Law and Law [14]. In the last study that uses activation-energy, asymptotic analysis for the isothermal, flat-plate boundary layer, the reacting flow is shown to be locally similar in the limit of large activation energy. Using this subsonic scaling of the ignition distance to analyze the laminar, supersonic, boundary-layer flows would result in very large ignition distances; however, this assessment does not account for the effects of viscous heating

3

in the supersonic flow that shorten the ignition distance. In fact, viscous heating is the primary source of heat that induces ignition in an adiabatic system. Jackson and Hussaini [11] studied the effect of viscous heating in their asymptotic study of a supersonic mixing layer. Later Ju and Niioka [13] extended that analysis to include multi-step chemistry. In both of these studies, a small viscous heating effect is assumed. Grosch and Jackson [9] extended the mixing layer results to include larger viscous-heating effects, and also considered finite activation energies. Again, the importance of viscous heating effects is shown by Figueira *et al.* [8] in their numerical study of supersonic, flat-plate, boundary-layer ignition with hydrogen-air chemistry. All of these studies concluded that the ignition distance reduces significantly when the effects of viscous heating are included in the analysis. Physically, the kinetic energy of the supersonic flow is converted into thermal energy through viscous heating in the boundary layer, thus the temperature rises and thereby accelerates the chemical reaction.

Im, Bechtold and Law [10] performed a numerical and asymptotic study of the weakly-reactive, laminar, supersonic, flat-plate, boundary-layer flow with $O(1)$ viscous heating and with a simplified, one-step, chemical-reaction model. They assumed constant physical properties, such as the specific heat and the density-weighted mass-diffusion coefficients. They also used unity values for the Lewis and Prandtl numbers. The study considered the weakly-reactive states through which ignition evolves from an initially frozen state. The inert solution provides the initial condition at the lead-

4

ing edge of the plate for the numerical calculations and represents the leading-order

temperature and concentration profiles for the asymptotic analysis. They described

the flow structure under various ignition situations and provided explicit expressions

for the ignition distance. The effects of the various physical parameters on the igni-

tion distance are assessed. They also showed that the ignition characteristics of the

boundary-layer flow depend significantly on the viscous heating term appearing in the

energy equation for supersonic flows. Two of the well-known mathematical models

that relate viscosity and temperature are the power law

$$\mu = T^s, \qquad 0.5 \leq s \leq 1 \qquad\qquad (1.0.1)$$

and Sutherland's model

$$\mu = \frac{a\,T^{\frac{3}{2}}}{b+T} \qquad\qquad (1.0.2)$$

where a and b are empirically determined constants. Sutherland's law is a better ap-

proximation for most gases and provides a more rapid variation of μ with respect to T

than the linear temperature-viscosity law (see [1]). By using the linear temperature-

viscosity law, $s = 1$ in the power law, the mathematical equations for the supersonic,

flat-plate, boundary-layer flow are such that the momentum equation is solved inde-

pendently of the energy equation. By using Sutherland's temperature-viscosity law,

the momentum and energy equations are coupled.

The present study extends the analysis of Im *et al.* [10] to a more general problem

concerning ignition analysis in the boundary layer behind a propagating, laminar

shock front. The present study uses Sutherland's temperature-viscosity law rather

5

than the linear temperature-viscosity law. A schematic of the problem is shown in Figure 1.1 showing the boundary layer formed behind a normal shock front moving with constant velocity u_s into a fluid at rest. The state of the gas behind the shock front, but outside of the boundary layer, is denoted by the subscript ∞. For a general review of shock waves, see [2].

1.1   Thesis Outline

The remainder of the thesis is organized as follows: In chapter two, non-dimensional equations are given for unsteady motion of a compressible gas in the boundary layer to leading order in a Reynolds number expansion. The choice is presented of the units of temperature, velocity, pressure, time, and length used to obtain the dimensionless independent variables. The equations are transformed through the Howarth-Dorodnitsyn transformation; then, a similarity variable is introduced to obtain a final closed system of equations for the unknowns u, ρ, T and Y. The derivations of the inert-stage momentum, energy and mass-fraction equations are contained in chapter three. The solution to these equations is determined numerically for both the adiabatic boundary conditions, with no transfer of heat across the wall, and the isothermal boundary conditions, with the wall temperature held constant. The results are discussed and presented graphically. Included in chapter four is the asymptotic analysis of the momentum and energy equations. The reaction zone analysis of the adiabatic wall is presented, and the momentum and energy equations for the outer region are

6

derived. The boundary conditions needed to solve these outer-region equations are determined from matching the inner and outer solutions. In chapter five, the solution to the coupled momentum and energy equations for the outer region are numerically determined by using the Crank-Nicolson algorithm. The results are presented graphically. The reaction-zone analysis for the isothermal wall is presented in chapter six, and the momentum and energy equations for the outer region are derived. The boundary conditions needed to solve the outer-region equations are again determined through matching the inner and outer solutions. In chapter seven, the solution to the outer-region momentum and energy equations for the isothermal wall are numerically determined by using the Crank-Nicolson algorithm. Concluding remarks are included in chapter eight. The appendices include details of the analysis that are either non-standard or not necessarily obvious.

7
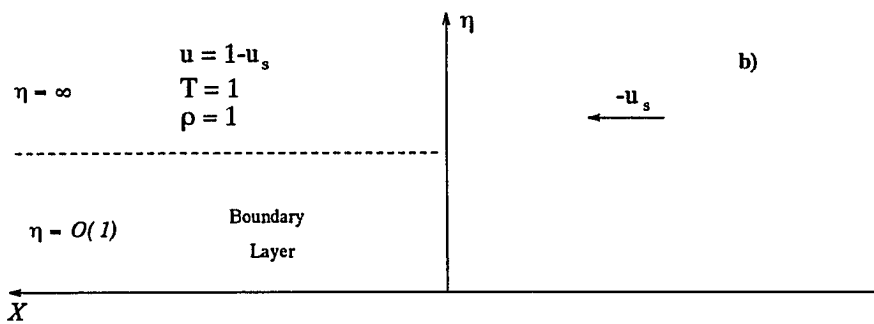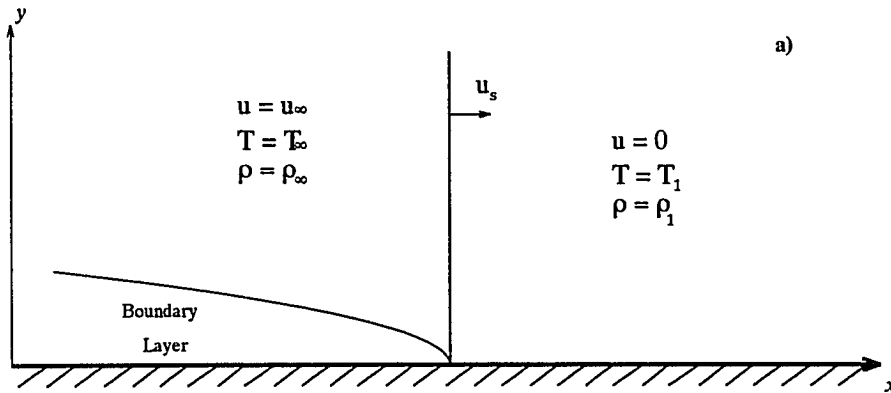
Figure 1.1: Schematic of the problem. a) Dimensional units in a frame of reference with the shock moving into a quiescent gas. b) Non-dimensional units and similarity variable in frame of reference with shock stationary.

8

Chapter 2

GOVERNING EQUATIONS

2.1 Boundary Layer Equations

The non-dimensional equations to the leading order in a Reynolds number expansion that govern the two-dimensional, unsteady motion of a compressible, reacting gas in the boundary layer are given by:

Continuity Equation

$$\rho_t + (\rho u)_x + (\rho \hat{v})_{\hat{y}} = 0, \qquad (2.1.1)$$

Momentum Equation

$$\rho[u_t + u u_x + \hat{v} u_{\hat{y}}] + \frac{1}{\gamma M^2} P_x = (\mu u_{\hat{y}})_{\hat{y}}, \qquad (2.1.2)$$

9

Energy Equation

$$\rho[T_t + uT_x + \hat{v}T_{\hat{y}}] - \frac{\gamma - 1}{\gamma}(P_t + uP_x) =$$

$$\frac{1}{P_r}(\mu T_{\hat{y}})_{\hat{y}} + (\gamma - 1)M^2\mu(u_{\hat{y}})^2 + \beta\Omega, \qquad (2.1.3)$$

Mass-Fraction Equation

$$\rho[Y_t + uY_x + \hat{v}Y_{\hat{y}}] = \frac{1}{P_r L_e}(\mu Y_{\hat{y}})_{\hat{y}} - \Omega, \qquad (2.1.4)$$

and

Equation of State

$$P = \rho T. \qquad (2.1.5)$$

T is the temperature, ρ is the density, P is the pressure and Y is the mass fraction of the deficient reactant in the combustible gas. The reaction is modeled as a simple, single-step, irreversible reaction.

The x-axis is taken in the direction of the flow and tangent to the wall; the y-axis is normal to the wall. The velocity component u is tangential to the wall, and $\hat{v}$ is the properly scaled component normal to the wall. In the derivation of the above system of equations, the rescaled boundary-layer variables

$$y = \frac{1}{\sqrt{R_e}}\hat{y} \qquad and \qquad v = \frac{1}{\sqrt{R_e}}\hat{v}. \qquad (2.1.6)$$

have been introduced in order to study the effects of chemistry in the boundary layer. Balancing the $v-$momentum equation, it is determined that to the leading order in the boundary layer, the pressure is a function of x and t.

10

The dimensionless variables are obtained by selecting T_0', Y_0', L_0'/u_0', $\rho_0' R T_0'$, and L_0' to be the units of temperature, mass fraction, time, pressure and length respectively. For convenience, T_0', ρ_0' and u_0' are chosen to be the freestream values behind the shock and are also denoted by T_∞', ρ_∞' and u_∞'. Thus $M = u_\infty'/a_\infty'$ is the Mach number of the gas (piston) pushing the shock front, and a_∞' is the speed of sound in the gas behind the shock front. The remaining non-dimensional quantities are the Prandtl number

$$P_r = \frac{\mu_0' c_p'}{k_0'},\tag{2.1.7}$$

the ratio of specific heat of a gas at constant pressure to that at constant volume γ, and the Reynolds number R_e

$$R_e = L_0'/(\frac{\mu_0'}{u_0' \rho_0'}) \quad \gg 1.\tag{2.1.8}$$

The heat release parameter β and the reaction term Ω are

$$\beta = \frac{Q' Y_0'}{c_p' T_0'}\tag{2.1.9}$$

and

$$\Omega = D \rho Y e^{-E/T}\tag{2.1.10}$$

where $E = E'/R^0 T_0'$ is the activation energy and $D = L_0'/u_0' D' = t_0' D'$ is the Damkohler number, with D' being the pre-exponential factor. Presently, the parameter D is arbitrary and making a choice implies a choice of the length scale. If D is

11

$O(1)$, then $\Omega \to 0$ in the limit $E \to \infty$, and the reaction term is zero to all algebraic orders. This suggests that D be chosen as

$$D = D_0 \epsilon^{\delta} e^{E/T^*} \tag{2.1.11}$$

where D_0, δ, and T^* are determined later in the analysis. The length scale of the problem is now given as

$$L_0' = \frac{u_0'}{D'} D_0 \epsilon^{\delta} e^{E/T^*}. \tag{2.1.12}$$

It is noted that the expression for D does not determine the characteristic length until the temperature T^* has been specified. If $T^* > 1$, the characteristic length is much shorter than the outer explosion distance (i.e., the distance between the shock and an insulated piston at thermal runaway; see [12]). In addition, if the distance between the shock and the piston face is much greater than the thickness of the boundary layer, the chemical effects are initially confined to the boundary layer with the outer flow being essentially inert. This allows the study of the "steady state" which develops in the boundary layer directly behind the shock. For a general discussion of activation energy asymptotics, see [3].

2.2   Variable Transformations

The mean flow equations (2.1.1) - (2.1.5) are first transformed to the incompressible equations by means of the Howarth-Dorodnitsyn transformation through the change

of variables

$$\xi = \int_0^y \rho(x, y', t) dy',$$ (2.2.13)

$$\bar{x} = x,$$ (2.2.14)

and

$$\bar{t} = t.$$ (2.2.15)

Then another change of variables is introduced

$$\eta = \frac{\sqrt{u_s}\xi}{\sqrt{u_s \bar{t} - \bar{x}}},$$ (2.2.16)

$$X = u_s \bar{t} - \bar{x},$$ (2.2.17)

and

$$\bar{\bar{t}} = \bar{t}.$$ (2.2.18)

where η is the similarity variable. The transformation in X means that the equations

are relative to a new coordinate system in which the shock front is stationary and the

fluid moves towards the shock front at a constant speed u_s. This speed u_s is found

in terms of the Mach number M of the piston speed to be

$$u_s = \frac{(3 - \gamma)M + \sqrt{(\gamma + 1)^2 M^2 + 16}}{4M}.$$ (2.2.19)

This relation is derived from Rankine-Hugoniot conditions (see appendix A). Fig-

ure 2.1 shows the shock speed u_s versus the Mach number M. Note that $u_s \to \infty$

as $M \to 0$, and for large M, the shock speed $u_s \to 1$. In reality, u_s measures the

speed of a traveling discontinuity that is initiated by the instantaneous movement

13

of the piston. This discontinuity is not formally a shock wave unless the speed of the discontinuity is greater than the speed of sound in the undisturbed gas. This condition for a formal shock wave to exist is equivalent to $M > 1$. Also, it is known that a small disturbance in the limit of zero Mach number travels at the speed of sound; the asymptotic relation $u_s \sim 1/M$ as $M \to 0$ is consistent with this fact since in dimensional units this asymptotic relation gives $u_s'/u_\infty' \sim a_\infty'/u_\infty'$.

Assuming that the pressure is constant, then $P(x,t) = 1$, and the transformations (2.2.13) and (2.2.18) yield

Continuity Equation

$$\frac{-u_s\eta}{2X}\frac{\partial\rho}{\partial\eta} + u_s\frac{\partial\rho}{\partial X} + \frac{\partial\rho}{\partial\bar{t}} + \frac{\partial\xi}{\partial t}\sqrt{\frac{u_s}{X}}\frac{\partial\rho}{\partial\eta}$$
$$+ \frac{\eta}{2X}\frac{\partial(\rho u)}{\partial\eta} - \frac{\partial(\rho u)}{\partial X} + \frac{\partial\xi}{\partial x}\sqrt{\frac{u_s}{X}}\frac{\partial(\rho u)}{\partial\eta} + \rho\sqrt{\frac{u_s}{X}}\frac{\partial(\rho\hat{v})}{\partial\eta} = 0, \qquad (2.2.20)$$

Momentum Equation

$$\frac{-u_s\eta}{2X}\frac{\partial u}{\partial\eta} + u_s\frac{\partial u}{\partial X} + \frac{\partial u}{\partial\bar{t}} + \frac{\partial\xi}{\partial t}\sqrt{\frac{u_s}{X}}\frac{\partial u}{\partial\eta}$$
$$+ u[\frac{\eta}{2X}\frac{\partial u}{\partial\eta} - \frac{\partial u}{\partial X} + \frac{\partial\xi}{\partial x}\sqrt{\frac{u_s}{X}}\frac{\partial u}{\partial\eta}] + \rho\hat{v}\sqrt{\frac{u_s}{X}}\frac{\partial u}{\partial\eta} = \frac{u_s}{X}\frac{\partial^2 u}{\partial\eta^2}, \qquad (2.2.21)$$

Energy Equation

$$\frac{\partial T}{\partial\bar{t}} - \frac{u_s\eta}{2X}\frac{\partial T}{\partial\eta} + u_s\frac{\partial T}{\partial X} + \frac{\partial\xi}{\partial t}\sqrt{\frac{u_s}{X}}\frac{\partial T}{\partial\eta}$$
$$+ u[\frac{\eta}{2X}\frac{\partial T}{\partial\eta} - \frac{\partial T}{\partial X} + \frac{\partial\xi}{\partial x}\sqrt{\frac{u_s}{X}}\frac{\partial T}{\partial\eta}] + \rho\hat{v}\sqrt{\frac{u_s}{X}}\frac{\partial T}{\partial\eta}$$
$$= \frac{1}{P_r}\frac{u_s}{X}\frac{\partial^2 T}{\partial\eta^2} + (\gamma - 1)M^2\frac{u_s}{X}(u_\eta)^2 + \frac{\beta}{\rho}\Omega, \qquad (2.2.22)$$

and

14

Mass-Fraction Equation

$$\frac{\partial Y}{\partial \bar{t}} - \frac{u_s \eta}{2X}\frac{\partial Y}{\partial \eta} + u_s\frac{\partial Y}{\partial X} + \frac{\partial \xi}{\partial t}\sqrt{\frac{u_s}{X}}\frac{\partial Y}{\partial \eta} + u[\frac{\eta}{2X}\frac{\partial Y}{\partial \eta} - \frac{\partial Y}{\partial X}$$

$$+ \frac{\partial \xi}{\partial x}\sqrt{\frac{u_s}{X}}\frac{\partial Y}{\partial \eta}] + \rho\hat{v}\sqrt{\frac{u_s}{X}}\frac{\partial Y}{\partial \eta} = \frac{1}{P_r L_e}\frac{u_s}{X}\frac{\partial^2 Y}{\partial \eta^2} - \frac{1}{\rho}\Omega. \qquad (2.2.23)$$

In the equations (2.2.20) - (2.2.23), the quantities ξ_t, ξ_x and $\xi_x u$ are

$$\xi_t = \int_0^\eta \{\xi_t \frac{\rho'_\eta}{\rho} - \frac{1}{2}\sqrt{\frac{u_s}{X}}\frac{\eta'\rho_{\eta'}}{\rho} + u_s\sqrt{\frac{X}{u_s}}\frac{\rho_X}{\rho} + \sqrt{\frac{X}{u_s}}\frac{\rho_{\bar{t}}}{\rho}\}d\eta', \qquad (2.2.24)$$

$$\xi_x = \int_0^y \{\frac{1}{2}\frac{1}{\sqrt{u_s X}}\frac{\eta'\rho_{\eta'}}{\rho} - \sqrt{\frac{X}{u_s}}\frac{\rho_X}{\rho} + \xi_x\frac{\rho_{\eta'}}{\rho}\}d\eta', \qquad (2.2.25)$$

and

$$\xi_x u = \int_0^\eta \{\frac{1}{2}\frac{u}{\sqrt{u_s X}}\frac{\eta'\rho_{\eta'}}{\rho} - u\sqrt{\frac{X}{u_s}}\frac{\rho_X}{\rho} + u\xi_x\frac{\rho_{\eta'}}{\rho} + \xi_x u_{\eta'}\}d\eta'. \qquad (2.2.26)$$

The derivation of the above relations is given in appendix B. The continuity equation (2.2.20) is solved for $(\rho\hat{v})_\eta$ and both sides integrated with respect to η to get $\rho\hat{v}$. Simplifying by use of equations (2.2.24) and (2.2.26) yields

$$\rho\hat{v} = -\xi_t - \xi_x u - \frac{1}{\sqrt{u_s X}}\int_0^\eta \frac{1}{2}\eta' u_{\eta'} d\eta' + \sqrt{\frac{X}{u_s}}\int_0^\eta u_X d\eta'. \qquad (2.2.27)$$

Using this expression, the momentum, energy, and mass-fraction equations (2.2.21), (2.2.22) and (2.2.23) are

Momentum Equation

$$u_{\bar{t}} + (u_s - u)u_X - \frac{u_s \eta}{2X}u_\eta + \frac{u_\eta}{2X}\int_0^\eta u d\eta' + u_\eta\int_0^\eta u_X d\eta' = \frac{u_s}{X}(\mu\rho u_\eta)_\eta, \qquad (2.2.28)$$

15

Energy Equation

$$T_{\tilde{t}} + (u_s - u)T_X - \frac{u_s\eta}{2X}T_\eta + \frac{T_\eta}{2X}\int_0^\eta u\,d\eta' + T_\eta \int_0^\eta u_X\,d\eta' =$$

$$\frac{1}{P_r}\frac{u_s}{X}(\mu\rho T_\eta)_\eta + (\gamma - 1)M^2\frac{u_s}{X}(\mu\rho)(u_\eta)^2 + \frac{\beta}{\rho}\Omega, \qquad (2.2.29)$$

and

Mass-Fraction Equation

$$Y_{\tilde{t}} + (u_s - u)Y_X - \frac{u_s\eta}{2X}Y_\eta + \frac{Y_\eta}{2X}\int_0^\eta u\,d\eta' + Y_\eta \int_0^\eta u_X\,d\eta' =$$

$$\frac{1}{P_r L_e}\frac{u_s}{X}(\mu\rho Y_\eta)_\eta - \frac{1}{\rho}\Omega. \qquad (2.2.30)$$

which along with the equation of state

$$\rho T = 1 \qquad (2.2.31)$$

provide a closed system for the unknowns u, ρ, T and Y.

16
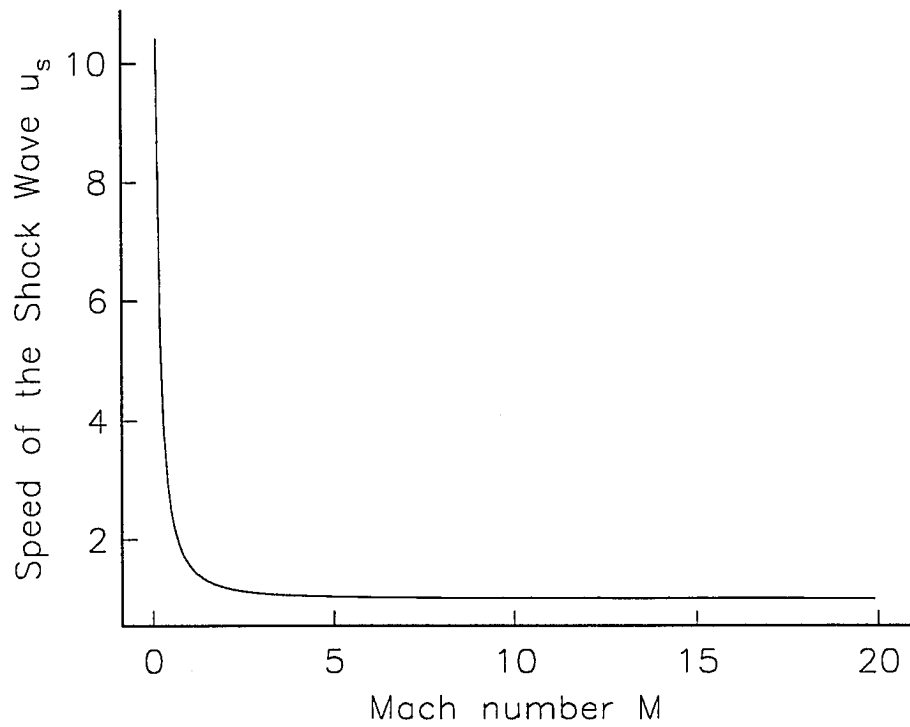
Figure 2.1: Speed of shock wave u_s as a function of Mach number M from Rankine-Hugoniot conditions.

17

Chapter 3

INERT STATE

3.1 Introduction

In the flow behind the shock front, there exists an inert heating stage prior to the events that lead to ignition. In this inert state, the flow is self-similar and it is assumed that the solution is independent of X and t. To get the momentum and energy equations for the inert state, we let $u(\eta, X, \bar{\bar{t}}) = u_I(\eta)$, $T(\eta, X, \bar{\bar{t}}) = T_I(\eta)$ and $Y(\eta, X, \bar{\bar{t}}) = Y_I(\eta)$ in the equations (2.2.28), (2.2.29) and (2.2.30). The subscript I denotes the inert-state dependent variables. The streamfunction $f(\eta)$ is introduced by letting $u_I(\eta) = f'(\eta)$. The appropriate change of variables is used to transform the momentum equation to the form of Im et $al.$ [10]. The resulting nonlinear, coupled system of equations with known boundary conditions for both adiabatic and isothermal walls is numerically determined. The inert solution provides the leading-order temperature and velocity profiles for the asymptotic analysis of ignition. A

18

comparison to the model of Im *et al.* [10] is made.

3.2 Inert State Equations

The momentum and energy equations for the inert state are

$$u_{I\eta}[\int_0^\eta u_I d\eta' - u_s\eta] = 2u_s(\mu\rho u_{I\eta})_\eta \qquad (3.2.1)$$

and

$$\frac{1}{2}[\int_0^\eta u_I(\eta')d\eta' - u_s\eta]T_{I\eta} = \frac{u_s}{P_r}[\mu\rho T_{I\eta}]_\eta + u_s(\gamma-1)M^2[\mu\rho u_{I\eta}^2], \qquad (3.2.2)$$

subject to the boundary conditions

$$u_I(0) = 0, \quad u_I(\infty) = 1, \qquad (3.2.3)$$

$$T_I(\infty) = 1, \qquad (3.2.4)$$

$$T_I(0) = T_s \qquad \textit{for isothermal wall}, \qquad (3.2.5)$$

and

$$\frac{dT_I(0)}{d\eta} = 0 \qquad \textit{for adiabatic wall}. \qquad (3.2.6)$$

In the adiabatic case, the wall at $\eta = 0$ is insulated so that there is no transfer of heat

across that surface; whereas, in the isothermal case, the wall at $\eta = 0$ is held constant

at some temperature T_s. The mass-fraction equation is trivially solved subject to the

conditions $Y_I(\infty) = 1$ and $Y_{I\eta}(0) = 0$ to get

$$Y_I(\eta) = 1. \qquad (3.2.7)$$

19

Letting $u_I(\eta) = f'(\eta)$ and denoting $\mu\rho$ by $\bar{\mu}$, the momentum equation becomes

$$(f - u_s\eta)f'' = 2u_s(\bar{\mu}f'')_\eta, \qquad (3.2.8)$$

subject to

$$f(0) = 0, \qquad (3.2.9)$$

$$f'(0) = 0, \qquad (3.2.10)$$

and

$$f'(\infty) = 1. \qquad (3.2.11)$$

The energy equation (3.2.2) becomes

$$\frac{1}{2}[f(\eta) - u_s\eta]T_{I\eta} = \frac{u_s}{P_r}[\bar{\mu}T_{I\eta}]_\eta + u_s(\gamma - 1)M^2[\bar{\mu}f''^2], \qquad (3.2.12)$$

subject to the same boundary conditions as above.

The momentum equation (3.2.8) is not independent of the energy equation since the term $\bar{\mu}$ is a function of temperature. In case of Im *et al.* [10], the linear temperature-viscosity law is used ($\bar{\mu} = 1$); the momentum equation decouples from the energy equation; and the velocity field is determined independently.

For comparison, it is convenient to transform the equations to the form of Im *et al.* [10] using the change of variables

$$f - u_s\eta = -\sqrt{2u_s}F, \qquad (3.2.13)$$

and

$$\eta = \sqrt{2u_s}\bar{\eta}. \qquad (3.2.14)$$

20

The momentum equation is now

$$F\ddot{F} = -(\overline{\dot{\bar{\mu}}\ddot{F}}),$$ (3.2.15)

subject to

$$F(0) = 0,$$ (3.2.16)

$$\dot{F}(0) = u_s,$$ (3.2.17)

and

$$\dot{F}(\infty) = u_s - 1.$$ (3.2.18)

where $(\dot{\ })$ is for $\frac{d}{d\bar{\eta}}$.

Similarly, the energy equation for the inert state in terms of $\bar{\eta}$ is

$$-FT_{I\bar{\eta}} = \frac{1}{P_r}[\bar{\mu}(T_I)T_{I\bar{\eta}}]_{\bar{\eta}} + (\gamma - 1)M^2\bar{\mu}(T_I)\ddot{F}^2,$$ (3.2.19)

subject to

$$T_I(\infty) = 1,$$ (3.2.20)

$$\frac{dT_I(0)}{d\bar{\eta}} = 0 \qquad for \; adiabatic \; wall,$$ (3.2.21)

and

$$T_I(0) = T_s \qquad for \; isothermal \; wall.$$ (3.2.22)

We note here that the governing equations are identical to the governing equations of Im et $al.$ [10], except that they have $\dot{F}(0) = 0$ and $\dot{F}(\infty) = 1$ as the boundary conditions and $\bar{\mu} = 1$. For comparison, these governing equations are solved using the

21

boundary conditions of [10] and $\bar{\mu} = 1$. This is referred to as the linear temperature-viscosity law with $u_s = 0$ case. Also solved are these governing equations using the boundary conditions of [10] and $\bar{\mu}$ computed through Sutherland's temperature-viscosity law. This is referred to as the Sutherland's law with $u_s = 0$ case. The solution of the above system, using the boundary conditions (3.2.16) through (3.2.18) for $\bar{\mu} = 1$, is referred to as the linear temperature-viscosity law with $u_s \neq 0$ case, and the solution for $\bar{\mu}$ computed through Sutherland's temperature-viscosity law is referred to as the Sutherland's law with $u_s \neq 0$ case. The results of all the four cases with different sets of the physical parameters are discussed in the next section.

3.3   Numerical Solutions and Results

The coupled momentum and energy equations (3.2.15) and (3.2.19) are numerically solved using COLSYS for both adiabatic and isothermal boundary conditions with different values of the independent parameters like Mach number, surface temperature and Prandtl number. For comparison purposes, the inert-state problem for the linear temperature-viscosity law is also solved for different values of the independent parameters. In addition, the inert-state problems for both the Sutherland's law and the linear temperature-viscosity law are solved for the boundary conditions in [10]. Results for the adiabatic boundary conditions, where there is no transfer of heat across the surface at $\bar{\eta} = 0$, are shown in Figures 3.1 through 3.6. Figure 3.1 shows the temperature $T_I(\bar{\eta}) - 1$ versus $\bar{\eta}$ for various values of Mach number increasing from

$M = 0.5$ to $M = 5$ and unit Prandtl number. The speed of shock wave u_s is calculated from equation (2.2.19). Note that, as the Mach number increases, there is a corresponding increase in the maximum inert temperature occurring at the boundary near $\bar{\eta} = 0$ due to viscous heating. This quantity will be referred to as the adiabatic surface temperature T_{ad}. The thickness of this thermal layer in terms of the similarity variable $\bar{\eta}$ remains relatively constant.

The asymptotic analysis of ignition in chapter four shows that $\ddot{T}_I(0)$ is an important quantity. In Figure 3.2, $\ddot{T}_I(0)$ versus Mach number M shows the significant increase in the magnitude of the $\ddot{T}_I(0)$ for large Mach numbers. For comparison, the graph of $\ddot{T}_I(0)$ versus Mach number M is shown for the four different problems mentioned. Solid and dash curves show the results of using the Sutherland's temperature-viscosity law. The shock speed u_s has been calculated from equation (2.2.19) (solid curve) and has also been set to zero (dashed curve). The dotted and circle curves show the results of using the linear temperature-viscosity law with $u_s \neq 0$ and with $\dot{F}(0) = 0$ and $\dot{F}(\infty) = 1$; for brevity, this will hereafter be referred to as the $u_s = 0$ case. The magnitude of the second derivative of the inert-state temperature near the boundary for the Sutherland's viscosity law is significantly larger than for the linear temperature-viscosity law, especially for large Mach numbers. This indicates a more localized viscous heating. A similar comparison is shown in Figure 3.3 and Figure 3.4 by plotting the inert-state temperature $T_I(\bar{\eta}) - 1$ versus $\bar{\eta}$ for these four cases. The Mach number $M = 2.0$ is used for Figure 3.3, and $M = 5.0$ is used for Figure

23

3.4. The difference is more significant for a large Mach number. Note that, although the adiabatic wall-temperature is the same for a constant Mach number, changing from the linear temperature-viscosity law to the Sutherland's temperature-viscosity law and changing from $u_s = 0$ to the shock speed u_s calculated through the Rankine-Hugoniot relations localizes the viscous heating near the boundary. On this point alone, it is seen that the ignition results found here differ substantially from [10].

Figure 3.5 shows velocity $u_I(\eta)$ versus η for different values of the Mach number and unit Prandtl number. Figure 3.6 shows $u_I(\eta)$ versus η for Mach number $M = 5.0$ for the above four cases. The solid and dashed curves are for Sutherland's law with $u_s \neq 0$ and $u_s = 0$, respectively. The dotted and circle curves are for the linear temperature-viscosity law with $u_s \neq 0$ and $u_s = 0$, respectively. The graph shows no difference between the velocity profiles for the $u_s \neq 0$ case and the $u_s = 0$ case. This is quite interesting since it is the velocity profiles that govern the creation of thermal energy through viscous heating. The major differences in the results for the $u_s \neq 0$ case and the $u_s = 0$ case are due to the differences in the convective terms only. These differences show up in the temperature profiles as seen in Figure 3.3 and Figure 3.4. Along with the previous differences noted in the second derivative of the temperature at the wall surface, it is found that when $u_s \neq 0$ and the Mach number is relatively large, the temperature profile is broader than in the $u_s = 0$ case when each are considered using the appropriate similarity variable. This is the opposite of the behaviour found at the wall. It should be noted that a direct comparison is not

24

necessarily proper since, in the two cases, the similarity variables represent different quantities; however, the overlapping of the two velocity profiles in their respective variables merit the special mention given here.

The system of equations (3.2.15) and (3.2.19) are also solved for the isothermal boundary conditions where the surface temperature is kept at a constant temperature T_s. In the isothermal wall case, there are two varying parameters, namely, the Mach number M and the surface temperature T_s. The effects of both parameters are analyzed by keeping one of them constant and varying the other. Also, for comparison purposes, the problem is solved for the linear temperature-viscosity law and the effect of changing from u_s, calculated from the Rankine-Hugoniot conditions, to the $u_s = 0$ case. Figure 3.7 shows the temperature $T_I(\bar{\eta}) - 1$ versus $\bar{\eta}$ for different values of Mach numbers ranging from $M = 0.5$ to $M = 5.0$ with surface temperature $T_s = 1$ and unit Prandtl number. The speed u_s, of the shock front, is calculated from equation (2.2.19). The plot shows that the maximum temperature lies in the interior of the boundary layer and the maximum value increases as the Mach number increases. It also shows that the effect of the Mach number on the location of the maximum temperature is not very significant. Figure 3.8 is a plot of $T_I(\bar{\eta}) - 1$ versus $\bar{\eta}$, for fixed Mach number $M = 5.0$, surface temperature $T_s = 1.0$ and Prandtl number $P_r = 1.0$. Solid and dash curves show the results of using the Sutherland's temperature-viscosity law. The solid curve is for u_s calculated from equation (2.2.19) and the dashed curve is for the $u_s = 0$ case. The dotted and circle curves show the results of using the

25

linear temperature-viscosity law for the $u_s \neq 0$ case and the $u_s = 0$ case, respectively. The plot shows a shift in the position of the maximum temperature location between the $u_s \neq 0$ and the $u_s = 0$ cases. Figure 3.9 shows the temperature $T_I(\bar{\eta}) - 1$ versus $\bar{\eta}$ for fix Mach number $M = 5.0$ and with the surface temperature increasing from $T_s = 0.5$ to $T_s = 3.5$. The effect of the surface temperature T_s on temperature profiles is shown in Figure 3.10 for fixed Mach number $M = 2.5$. If the value of the surface temperature T_s is greater than the adiabatic value T_{ad}, then the temperature attains its maximum at the boundary $\bar{\eta} = 0$. Hence, the outer-region analysis for the isothermal wall, discussed in chapter six, fails. Figure 3.11 shows the velocity $u_I(\eta)$ versus η for different values of the Mach number. It is determined that the velocity profile does not vary much with the Mach number M. The effect of surface temperature on the velocity profiles is shown in Figure 3.12 for fixed Mach number $M = 5.0$. In Figure 3.13, velocity profiles for the Sutherland's and the linear temperature-viscosity law are shown. The solid curve denotes the use of the Sutherland's law and the dotted curve denotes the use of the linear law.
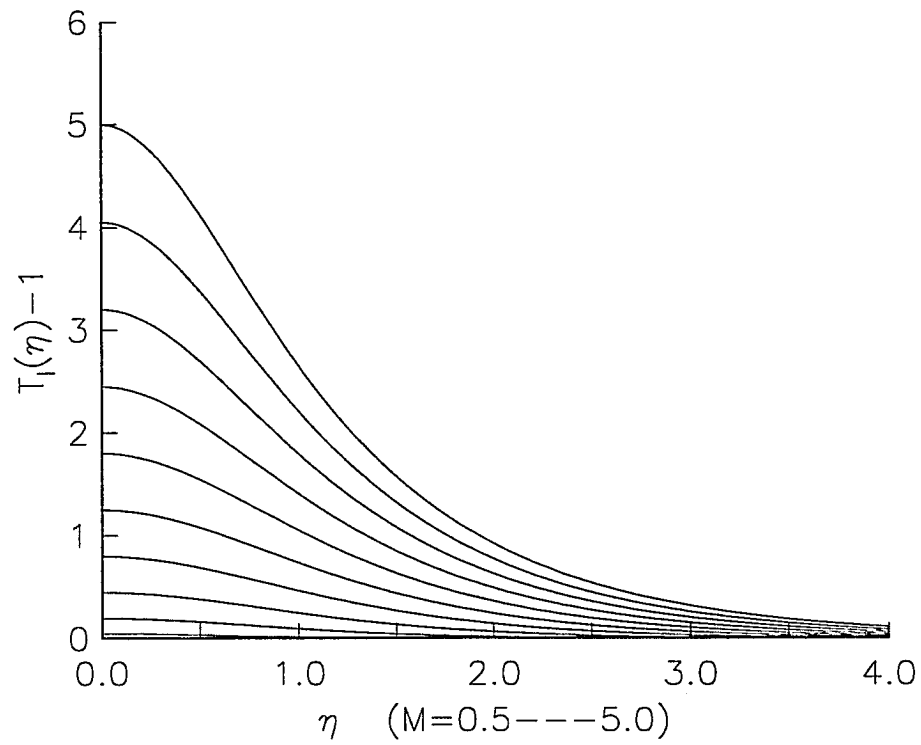
Figure 3.1: Mean flow temperature profiles for adiabatic wall for Mach number increasing from $M = 0.5$ to $M = 5.0$.

27
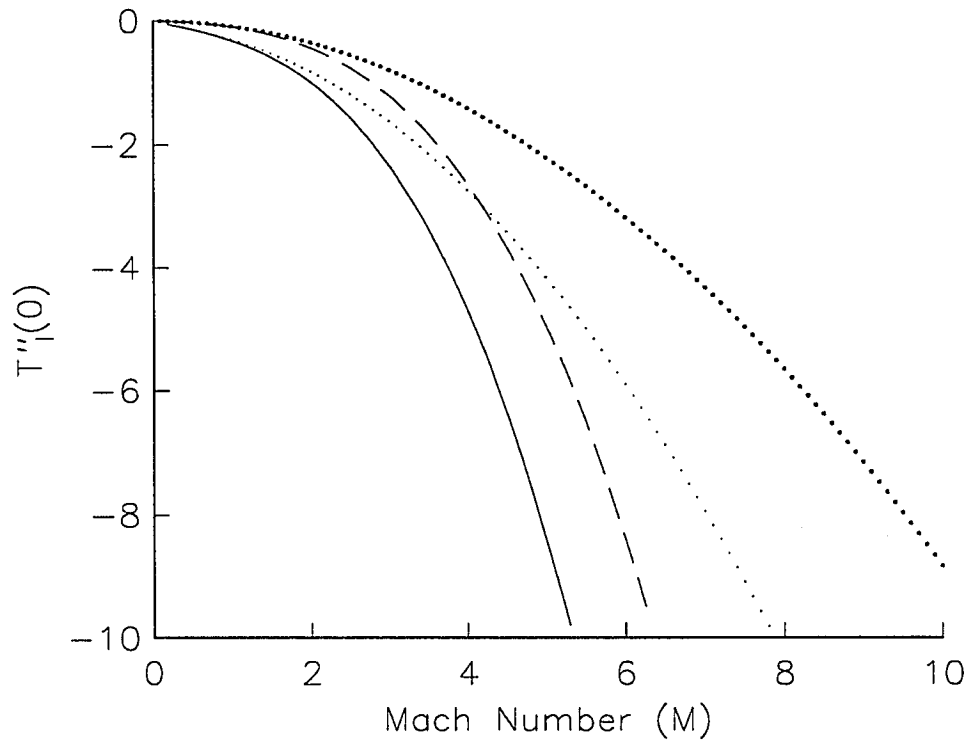
Figure 3.2: Plots of $\ddot{T}_I(0)$ versus Mach number M for adiabatic wall case. Solid curve for Sutherland's law with u_s calculated from Rankine-Hugoniot condition. Dashed curve for Sutherland's law with $u_s = 0$. Dotted and circle curves for linear law with $u_s \neq 0$ and $u_s = 0$, respectively.

28
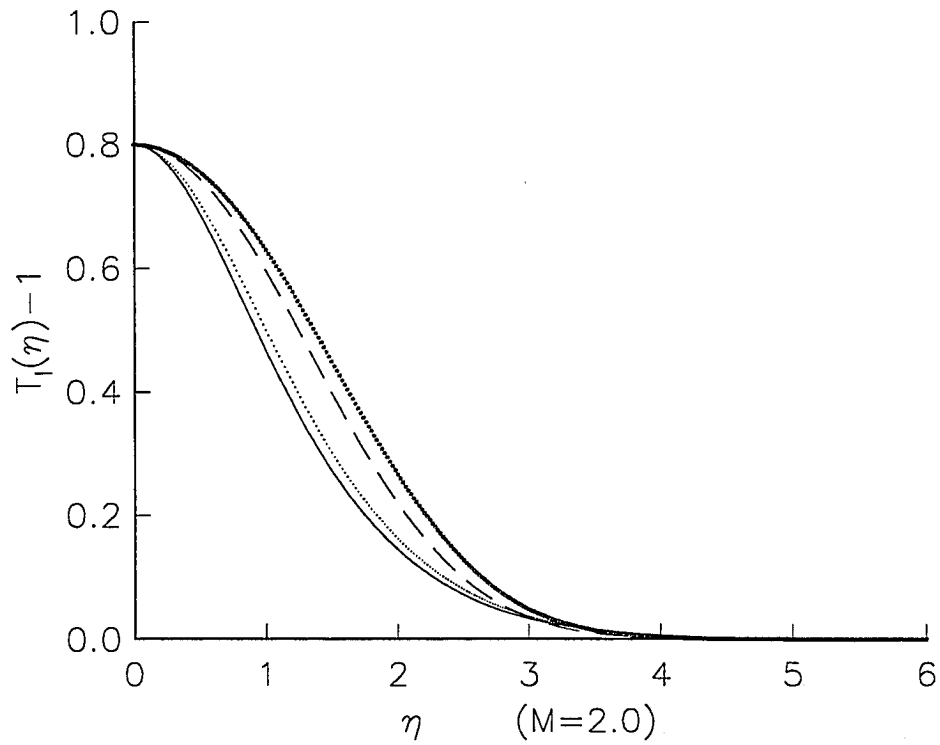
Figure 3.3: Mean flow temperature profiles for adiabatic wall. Solid and dashed curves for Sutherland's law with $u_s \neq 0$ and $u_s = 0$, respectively. Dotted and circle curves for linear law with $u_s \neq 0$ and $u_s = 0$, respectively. The value of Mach number used for these results is 2.0.

29
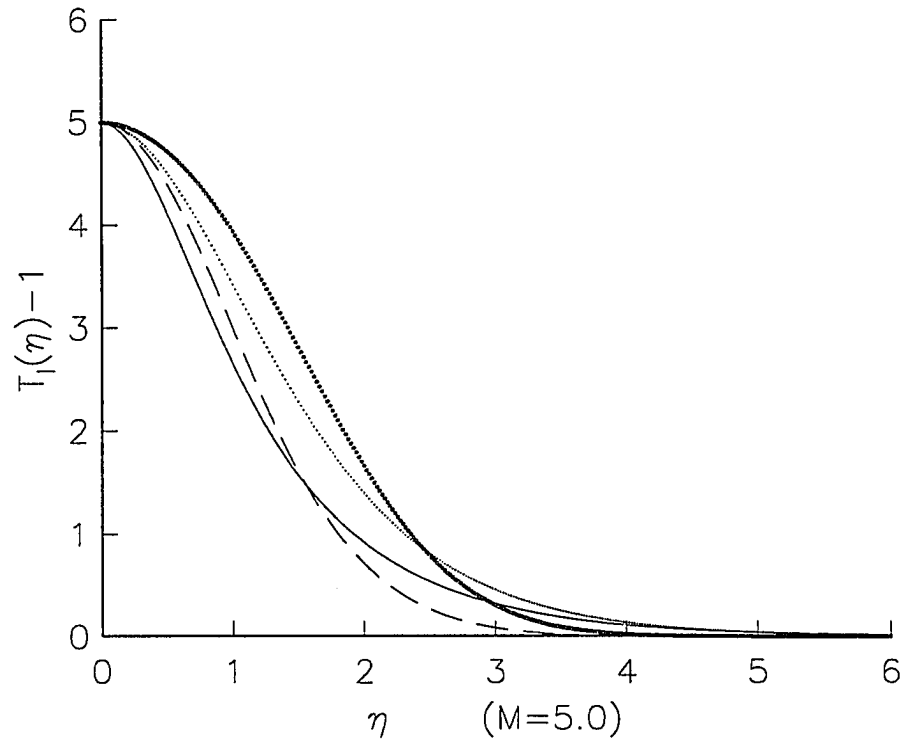
Figure 3.4: Mean flow temperature profiles for adiabatic wall. Solid and dashed curves for Sutherland's law with $u_s \neq 0$ and $u_s = 0$, respectively. Dotted and circle curves for linear law with $u_s \neq 0$ and $u_s = 0$, respectively. The value of Mach number used is 5.0.

30
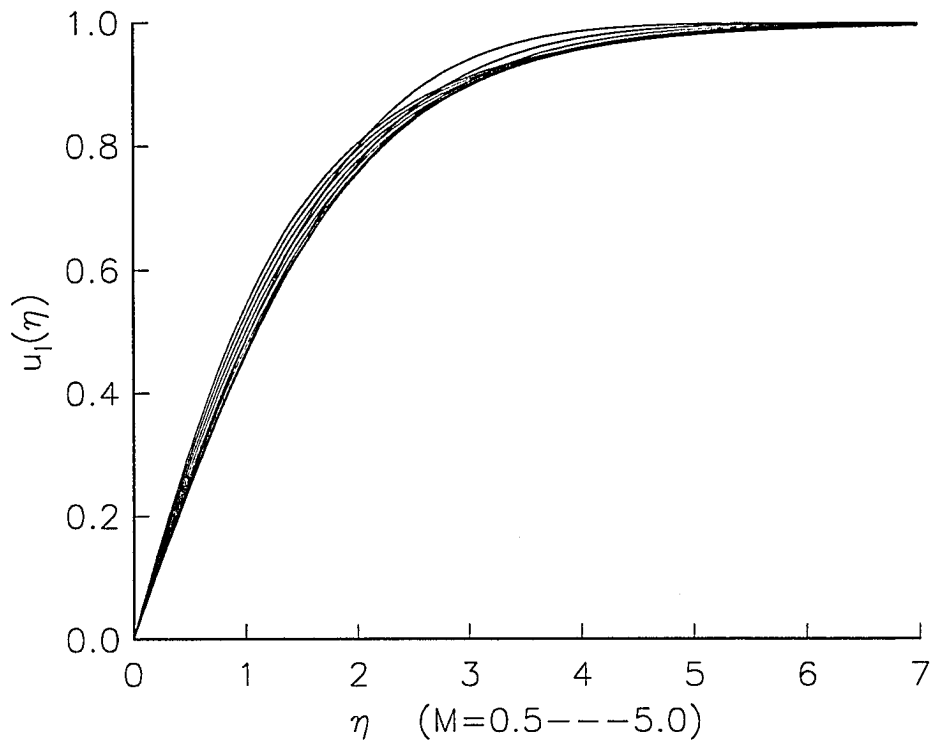
Figure 3.5: Mean flow velocity profile for adiabatic wall $u_I(\eta)$ versus η for Mach number increasing from $M = 0.5$ to $M = 5.0$.

31
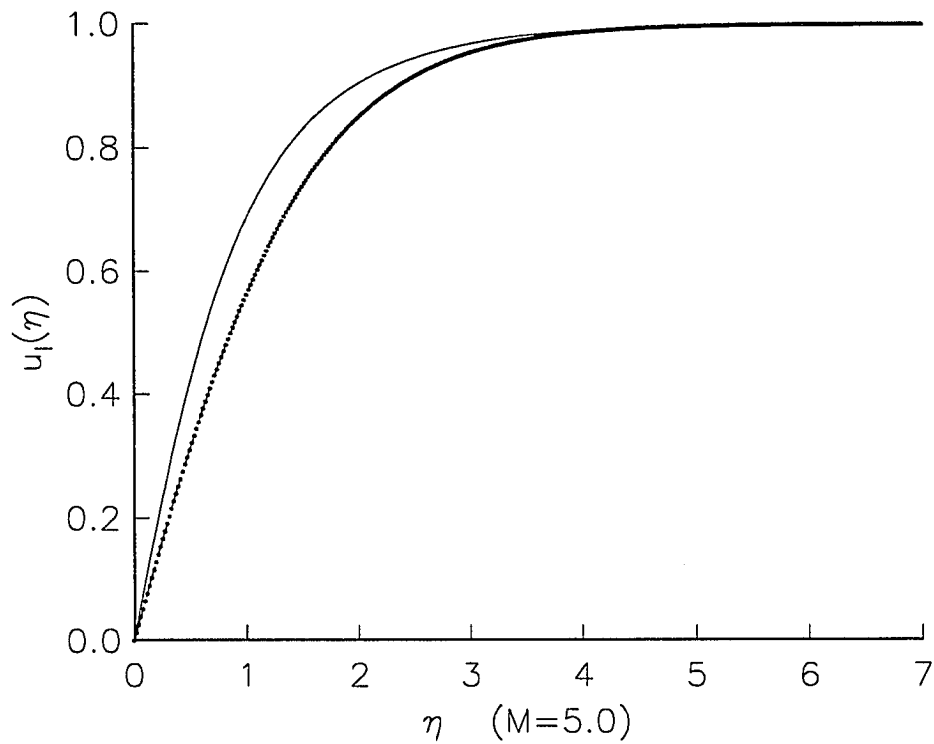
Figure 3.6: Mean flow velocity profiles for adiabatic wall $u_I(\eta)$ versus η for Mach number $M = 5.0$. Solid and dashed curves for Sutherland's law with $u_s \neq 0$ and $u_s = 0$, respectively. Dotted and circle curves for linear law with $u_s \neq 0$ and $u_s = 0$, respectively. There is no discernible difference between the mean flow velocity profiles for $u_s = 0$ and $u_s \neq 0$.

32
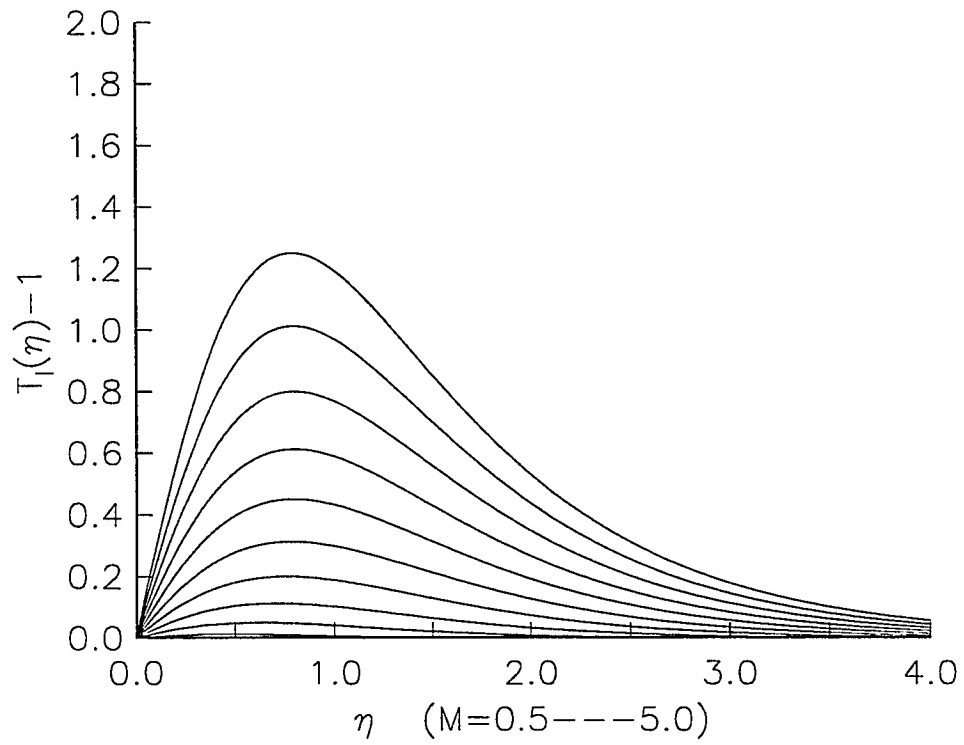
Figure 3.7: Mean flow temperature profiles for isothermal wall case for Mach number increasing from $M = 0.5$ to $M = 5.0$.

33
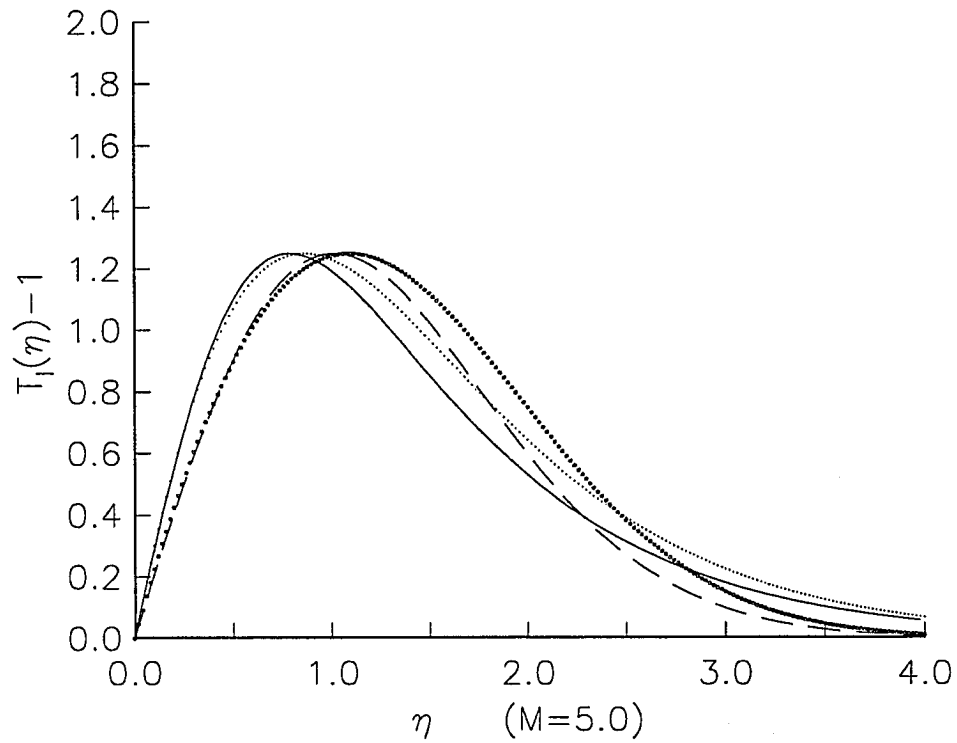
Figure 3.8: Mean flow temperature profile for isothermal wall. Solid and dashed curves for Sutherland's law with $u_s \neq 0$ and $u_s = 0$, respectively. Dotted and circle curves for linear law with $u_s \neq 0$ and $u_s = 0$, respectively. The value of Mach number used is 5.0 and the surface temperature $T_s = 1.0$.

34
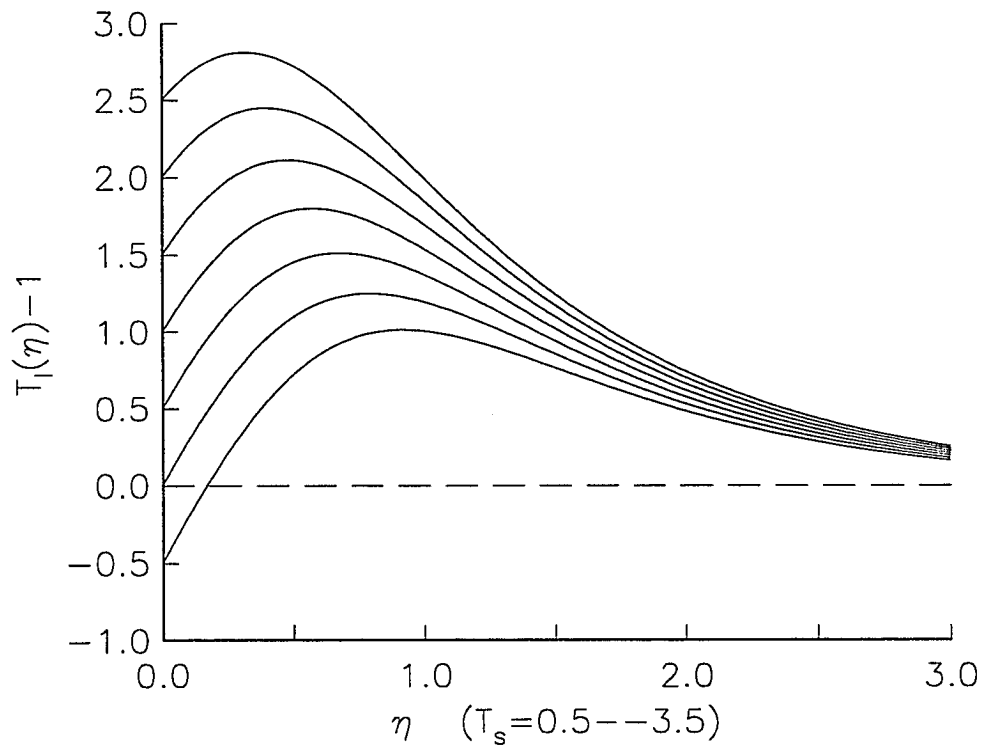
Figure 3.9: Mean flow temperature profiles for isothermal wall for fixed Mach number $M = 5.0$ and surface temperature increasing from $T_s = 0.5$ to $T_s = 3.5$.

35
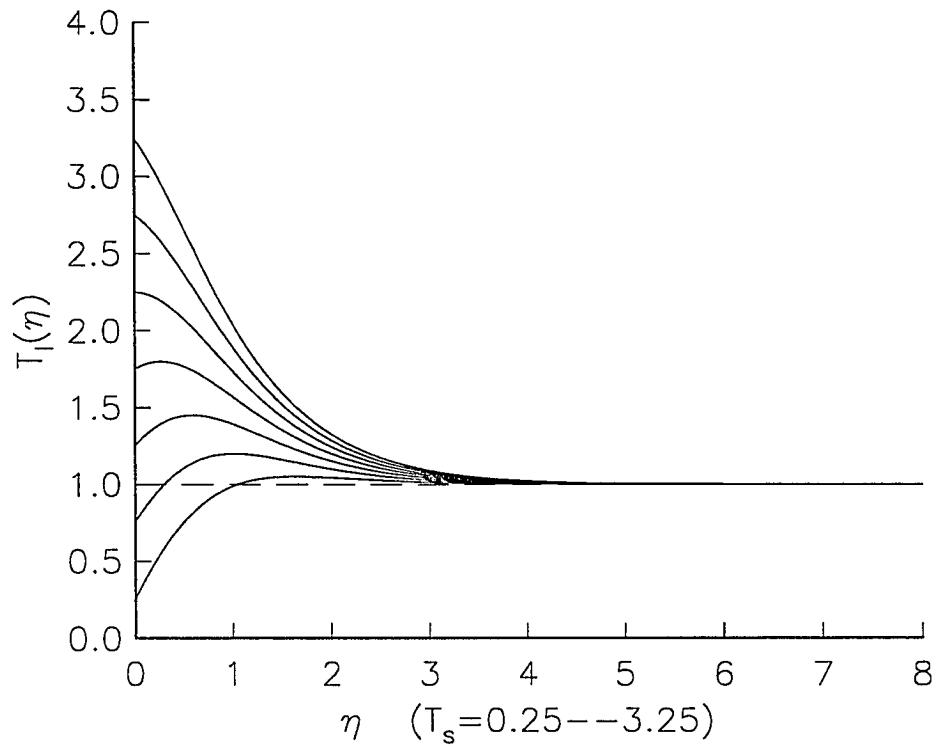
Figure 3.10: Mean flow temperature profiles for isothermal wall for fixed Mach number $M = 2.5$ and surface temperature increasing from $T_s = 0.25$ to $T_s = 3.25$.

36
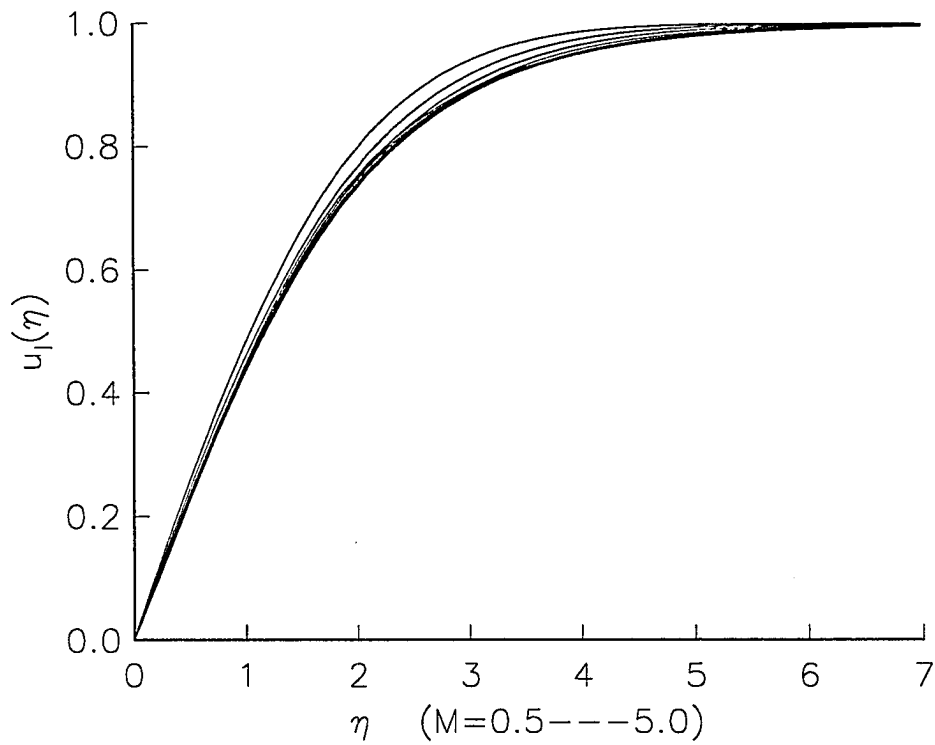
Figure 3.11: Mean flow velocity profile for isothermal wall $u_I(\eta)$ versus η for fixed surface temperature $T_s = 1.0$ and Mach number increasing from $M = 0.5$ to $M = 5.0$.

37
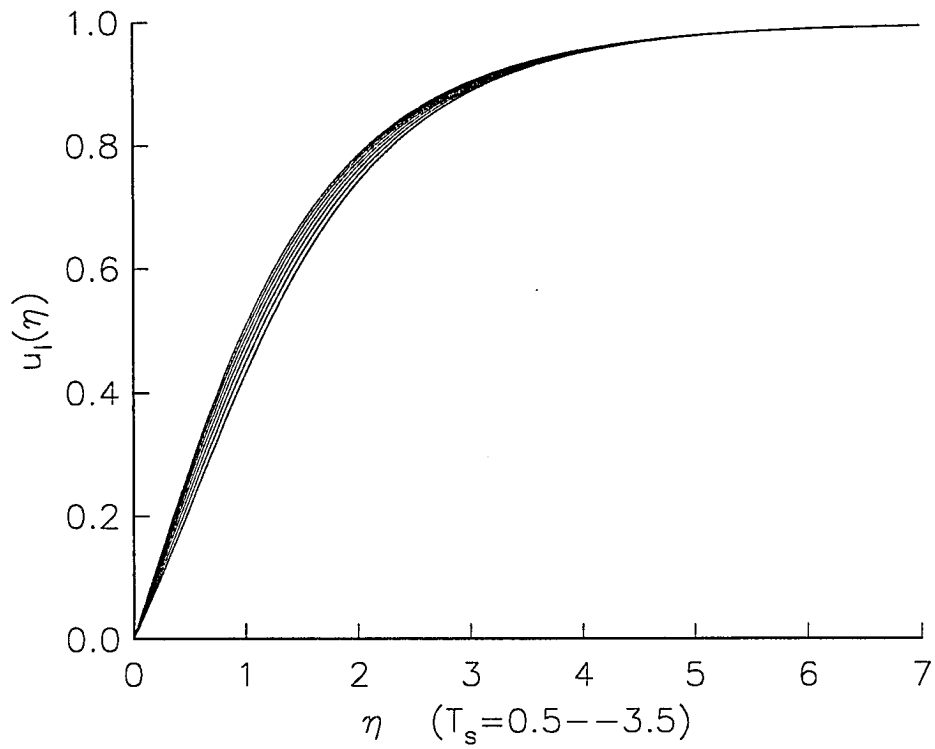
Figure 3.12: Mean flow velocity profile for isothermal wall $u_I(\eta)$ versus η for fixed Mach number $M = 5.0$ and surface temperature increasing from $T_s = 0.5$ to $T_s = 3.5$.

38
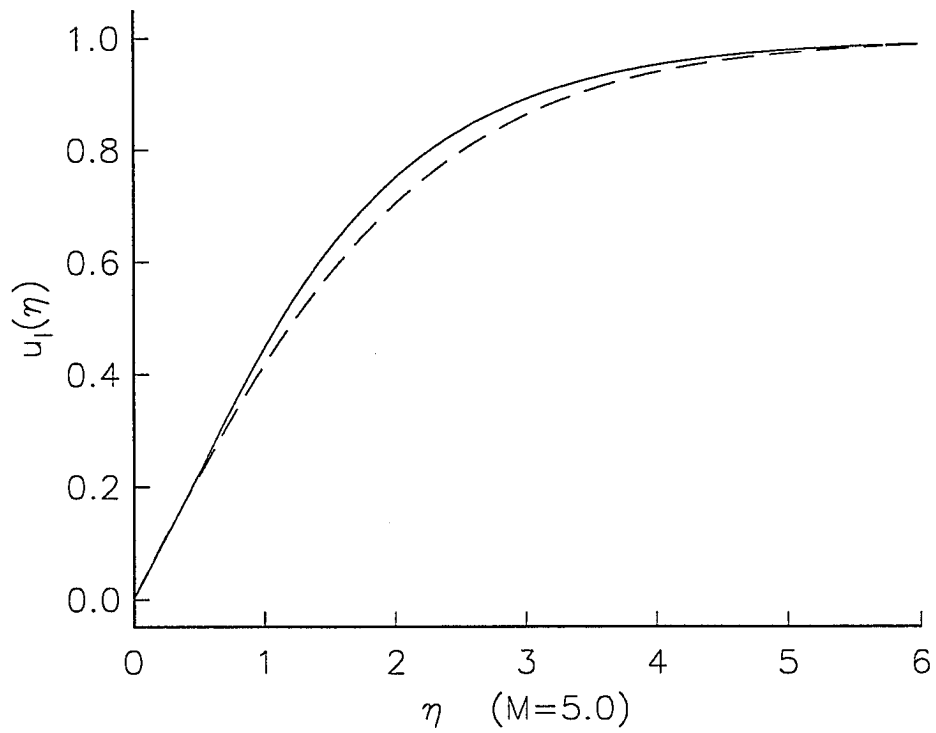
Figure 3.13: Mean flow velocity profiles for isothermal wall $u_I(\eta)$ versus η for Mach number $M = 5.0$. Solid curve for Sutherland's law, dashed curve for linear law.

39

Chapter 4

ANALYSIS OF THE

ADIABATIC WALL

4.1   Introduction

In this section, high activation-energy asymptotics is used to analyze the ignition process. Using the transformations (3.2.13) and (3.2.14), the momentum equation (2.2.28) and the energy equation (2.2.29) are transformed in terms of the variable $\bar{\eta}$ to get

$$2X(u_{\bar{\xi}} + (u_s - u)u_X) - u_s\bar{\eta}u_{\bar{\eta}}$$
$$+\frac{1}{\sqrt{2u_s}}u_{\bar{\eta}}\int_0^{\sqrt{2u_s\bar{\eta}}} u\,d\bar{\eta}' + \frac{2X}{\sqrt{2u_s}}u_{\bar{\eta}}\int_0^{\sqrt{2u_s\bar{\eta}}} u_X\,d\bar{\eta}' = (\mu\rho u_{\bar{\eta}})_{\bar{\eta}}, \qquad (4.1.1)$$

and

40

$$2X(T_{\bar{t}} + (u_s - u)T_X) - u_s\bar{\eta}T_{\bar{\eta}} + \frac{1}{\sqrt{2u_s}}T_{\bar{\eta}}\int_0^{\sqrt{2u_s\bar{\eta}}}u\,d\bar{\eta}'$$

$$+\frac{2X}{\sqrt{2u_s}}T_{\bar{\eta}}\int_0^{\sqrt{2u_s\bar{\eta}}}u_X\,d\bar{\eta}'$$

$$= \frac{1}{P_r}(\mu\rho T_{\bar{\eta}})_{\bar{\eta}} + (\gamma - 1)M^2(\mu\rho)(u_{\bar{\eta}})^2 + 2X\frac{\beta}{\rho}\Omega. \qquad (4.1.2)$$

The assumption is made that the reacting flow behind the shock front is steady in the frame of reference moving with the shock front; hence, the time dependence in the above equations will be dropped. As the distance from the shock increases, the terms in equation (4.1.2) multiplied by X become important. To analyze this process, introduce the perturbation of u, T, Y and $\bar{\mu}$ as

$$u = u_I(\bar{\eta}) + \epsilon\bar{u}_0(X,\bar{\eta};\epsilon) + O(\epsilon^2), \qquad (4.1.3)$$

$$T = T_I(\bar{\eta}) + \epsilon\Psi_0(X,\bar{\eta};\epsilon) + O(\epsilon^2), \qquad (4.1.4)$$

$$Y = Y_I(\bar{\eta}) + \epsilon Y_0(X,\bar{\eta};\epsilon) + O(\epsilon^2), \qquad (4.1.5)$$

and

$$\bar{\mu} = \bar{\mu}(T_I) + \epsilon\bar{\mu}'(T_I)\Psi_0(X,\bar{\eta};\epsilon) + O(\epsilon^2). \qquad (4.1.6)$$

The equations, valid through terms which are larger than $O(\epsilon^2)$, are

Perturbed Momentum Equation

$$2X\dot{F}\bar{u}_{0X} - F\bar{u}_{0\bar{\eta}} - (\bar{\mu}_I\bar{u}_{0\bar{\eta}})_{\bar{\eta}} =$$

$$-[\bar{\mu}_I'\ddot{F}\Psi_0]_{\bar{\eta}} + \frac{1}{\sqrt{2u_s}}\ddot{F}[\int_0^{\sqrt{2u_s\bar{\eta}}}\bar{u}_0\,d\bar{\eta}' + +2X\int_0^{\sqrt{2u_s\bar{\eta}}}\bar{u}_{0X}\,d\bar{\eta}'], \qquad (4.1.7)$$

and

Perturbed Energy Equation

$$2X\dot{F}\Psi_{0X} - F\Psi_{0\bar{\eta}} + \frac{1}{\sqrt{2u_s}}T_{I\bar{\eta}}[\int_0^{\sqrt{2u_s\bar{\eta}}}\bar{u}_0\,d\bar{\eta}' + 2X\int_0^{\sqrt{2u_s\bar{\eta}}}\bar{u}_{0X}\,d\bar{\eta}'] =$$

$$\frac{1}{P_r}[\bar{\mu}_I\Psi_{0\bar{\eta}} + \bar{\mu}_I'T_{I\bar{\eta}}\Psi_0]_{\bar{\eta}}$$

$$+(\gamma - 1)M^2[-2\ddot{F}\bar{\mu}_I\bar{u}_{0\bar{\eta}} + \bar{\mu}_I'\ddot{F}^2\Psi_0] + \frac{2X\beta}{\epsilon\rho}\Omega \qquad (4.1.8)$$

41

where the reaction term Ω will be expanded later. The functions $\bar{u}_0$ and Ψ_0 satisfy homogeneous boundary conditions, since the non-zero boundary conditions for momentum and temperature are completely satisfied by the leading-order terms of the asymptotic expansion, namely u_I and T_I. Therefore,

$$\bar{u}_0(0) = \bar{u}_0(\infty) = \Psi_0(0) = \Psi_0(\infty) = 0. \qquad (4.1.9)$$

4.2 Reaction Zone Analysis

The reaction term Ω in the perturbed energy equation (4.1.8) is sensitive to temperature variations, and a slight temperature rise is sufficient for ignition to occur on a much shorter time scale. The exponent in the reaction term suggests that, in the limit $E \to \infty$ being considered here, the reaction initiates near the hottest location in the inert-state flow field. For the adiabatic case, the reaction zone is near the wall (*i.e.*, near $\bar{\eta} = 0$). Expanding $T_I(\bar{\eta})$ near $\bar{\eta} = 0$ gives

$$T_I(\bar{\eta}) = T_{ad} + \frac{\bar{\eta}^2}{2}\frac{d^2 T_I(0)}{d\bar{\eta}^2} + \dots. \qquad (4.2.10)$$

meaning the inert-state profile has a parabolic shape and suggests that the inner structure is of $O(\sqrt{\epsilon})$ thickness. To examine the behaviour in the reaction zone, the inner, stretched variable ξ is introduced as

$$\bar{\eta} = \epsilon^{\frac{1}{2}}\xi. \qquad (4.2.11)$$

Note that the ξ used here is different from the ξ used before.

The expansions of the inert temperature, mass fraction, viscosity and streamfunction used in the forthcoming analysis are

$$T_I = T_{ad} + \epsilon\frac{\ddot{T}_I(0)}{2}\xi^2 + \dots, \qquad (4.2.12)$$

42

$$Y_I = 1, \tag{4.2.13}$$

$$\bar{\mu}(T_I) = \bar{\mu}(T_{ad}) + \epsilon\bar{\mu}'(T_{ad})\frac{\ddot{T}_I(0)}{2}\xi^2 + \dots, \tag{4.2.14}$$

$$\bar{\mu}'(T_I) = \bar{\mu}'(T_{ad}) + \epsilon\bar{\mu}''(T_{ad})\frac{\ddot{T}_I(0)}{2}\xi^2 + \dots, \tag{4.2.15}$$

$$F = \epsilon^{\frac{1}{2}}u_s\xi + \epsilon\frac{\ddot{F}(0)}{2}\xi^2 + \dots, \tag{4.2.16}$$

$$\dot{F} = u_s + \epsilon^{\frac{1}{2}}\ddot{F}(0)\xi + \epsilon\frac{1}{2}\frac{d^3F}{d\bar{\eta}^3}(0)\xi^2 + \dots, \tag{4.2.17}$$

and

$$\ddot{F} = \ddot{F}(0) + \epsilon^{\frac{1}{2}}\frac{d^3F}{d\bar{\eta}^3}(0) + \epsilon\frac{1}{2}\frac{d^4F}{d\bar{\eta}^4}(0)\xi^2 + \dots. \tag{4.2.18}$$

Substituting the transformation (4.2.11) and the expansions (4.2.12) through (4.2.18) into the perturbed momentum and energy equations (4.1.7) and (4.1.8) and keeping only $O(\epsilon^{-1/2})$ and lower-order terms gives

$$-\epsilon^{-1}\bar{\mu}(T_{ad})\bar{u}_{0\xi\xi} = -\epsilon^{-1/2}\bar{\mu}'(T_{ad})\ddot{F}(0)\Psi_{0\xi} \tag{4.2.19}$$

and

$$\epsilon^{-1}\frac{1}{P_r}[\bar{\mu}(T_{ad})\Psi_{0\xi}]_\xi = -\epsilon^{-1}\frac{2X\beta}{\rho}\Omega + \epsilon^{-1/2}2(\gamma-1)M^2\ddot{F}(0)\bar{\mu}(T_{ad})\bar{u}_{0\xi}, \tag{4.2.20}$$

which simplifies to

$$\bar{u}_{0\xi\xi} = \epsilon^{\frac{1}{2}}\frac{\bar{\mu}'(T_{ad})}{\bar{\mu}(T_{ad})}\ddot{F}(0)\Psi_{0\xi} \tag{4.2.21}$$

and

$$\Psi_{0\xi\xi} = \frac{-2XP_r}{\bar{\mu}(T_{ad})}\frac{\beta}{\rho}\Omega + \epsilon^{\frac{1}{2}}[2P_r(\gamma-1)M^2\ddot{F}(0)\bar{u}_{0\xi}]. \tag{4.2.22}$$

Of primary concern is the form of the reaction term under these assumptions. By definition,

$$
\begin{aligned}
\Omega &= D\rho Y e^{-E/T} \\
&= D_0\epsilon^\delta \rho Y e^{E[1/T^*-1/T]} \tag{4.2.23}
\end{aligned}
$$

43

where

$$D = D_0 \epsilon^\delta e^{\frac{E}{T^*}}. \tag{4.2.24}$$

The unknown quantities D_0, δ and T^* are chosen in the analysis below. The perturbation expansion for T from equation (4.1.4) is

$$
\begin{aligned}
T &= T_I + \epsilon \Psi_0(X, \bar\eta; \epsilon) + \dots \\
&= T_{ad} + \epsilon \{ \frac{\ddot{T}(0)}{2} \xi^2 + \Psi_0 \} + \dots.
\end{aligned}
\tag{4.2.25}
$$

Using this, the term $[1/T^* - 1/T]$ on the right-hand side of equation (4.2.23) for $T^* = T_{ad}$ simplifies to

$$\frac{1}{T^*} - \frac{1}{T} = \epsilon \frac{\Psi_0 + \frac{\ddot{T}(0)}{2}\xi^2}{T_{ad}^2}, \tag{4.2.26}$$

suggesting that, for convenience, the choice of ϵ should be

$$\epsilon = \frac{T_{ad}^2}{E} \tag{4.2.27}$$

where T_{ad} and E are the non-dimensional wall temperature and activation energy respectively. The exponential is now simplified as

$$e^{E[1/T^* - 1/T]} \approx e^{(\ddot{T}_I(0)\xi^2/2 + \Psi_0)}. \tag{4.2.28}$$

Using (4.2.28) in (4.2.22), the energy equation becomes

$$\Psi_{0\xi\xi} = -\epsilon^\delta \frac{2XP_r}{\bar\mu(T_{ad})} \beta D_0 e^{(\ddot{T}_I(0)\xi^2/2 + \Psi_0)} + \epsilon^{1/2}[2P_r(\gamma - 1)M^2 \ddot{F}(0)\bar{u}_{0\xi}]. \tag{4.2.29}$$

Achieving an asymptotic match with the outer solution requires that $\Psi_0(X, \xi)$ be expressed as

$$\Psi_0(X, \xi) = \bar\psi_0(X) + \epsilon^{1/2}\bar\psi_1(X, \xi), \tag{4.2.30}$$

and balancing terms in the momentum equation requires

$$\bar{u}_0(X, \xi) = u_0(X, \xi) + \epsilon^{1/2} u_1(X, \xi). \tag{4.2.31}$$

44

This governing system is now

$$u_{0\xi\xi} = 0, \tag{4.2.32}$$

$$u_{1\xi\xi} = 0, \tag{4.2.33}$$

and

$$\bar{\psi}_{1\xi\xi} = -\epsilon^{\delta-1/2} \frac{2P_r}{\bar{\mu}(T_{ad})} \beta D_0 X e^{\bar{\psi}_0(X)} e^{-b^*\xi^2} + P_r(\gamma-1)M^2 \ddot{F}(0)u_{0\xi} \tag{4.2.34}$$

where

$$b^* = \frac{-\ddot{T}_I(0)}{2}. \tag{4.2.35}$$

For the reaction term to be included in the analysis, $\delta = 1/2$ must be chosen. By choosing δ, T^* and for convenience $D_0 = 1$, the choice of a length scale for the original problem is complete.

Integrating equations (4.2.32) and (4.2.33) twice with respect to ξ and using the physical boundary condition at $\xi = 0$ gives

$$u_0(X, \xi) = A_1 \xi \tag{4.2.36}$$

and

$$u_1(X, \xi) = \bar{u}_1(X)\xi \tag{4.2.37}$$

where $\bar{\psi}_0(X)$ and $\bar{u}_1(X)$ remain unknown at this point, but are found later. Achieving an asymptotic match with the outer solution requires $A_1 \equiv 0$. Hence, the last term on the right-hand side of equation (4.2.34) is zero.

Integrating equation (4.2.34) twice with respect to ξ and using the result

$$\int_0^\xi \int_0^{\xi'} e^{-b^*\xi''^2} d\xi'' d\xi' \rightarrow \frac{\sqrt{\pi}}{2\sqrt{b^*}}\xi + \frac{1}{2b^*} - \frac{1}{b^*}e^{-b^*\xi^2} + \dots \quad as \quad \xi \rightarrow \infty \tag{4.2.38}$$

provides the relation for $\bar{\psi}_1$ in the limit as $\xi \rightarrow \infty$,

$$\bar{\psi}_1(X, \xi) \rightarrow -\frac{2P_r}{\bar{\mu}(T_{ad})}\beta X e^{\bar{\psi}_0(X)}\{\frac{1}{2b^*} + \frac{\sqrt{\pi}}{2\sqrt{b^*}}\xi\}. \tag{4.2.39}$$

45

The leading-order term $\bar{\psi}_0(X)$ is determined after matching the inner reaction-zone solution t o the outer non-reacting-zone solution. The equation (4.2.39) is written in a simplified form as

$$\bar{\psi}_1(X,\xi) \to A\xi + B \qquad as \qquad \xi \to \infty \tag{4.2.40}$$

where

$$A = -\frac{\bar{D}\sqrt{\pi}}{2\sqrt{b^*}} X e^{\bar{\psi}_0(X)}, \tag{4.2.41}$$

$$B = -\frac{\bar{D}}{2b^*} X e^{\bar{\psi}_0(X)}, \tag{4.2.42}$$

and

$$\bar{D} = \frac{2P_r\beta}{\bar{\mu}(T_{ad})}. \tag{4.2.43}$$

4.3 Analysis of the Outer Region

To analyze the problem in the outer frozen region, the expansions

$$u = u_I(\bar{\eta}) + \epsilon U(X,\bar{\eta}) + O(\epsilon^{3/2}) \tag{4.3.44}$$

and

$$T = T_I(\bar{\eta}) + \epsilon\Phi(X,\bar{\eta}) + O(\epsilon^{3/2}) \tag{4.3.45}$$

are used in the momentum equation (4.1.1) and the energy equation (4.1.2) to get

$$2X\dot{F}U_X - FU_{\bar{\eta}} - (\bar{\mu}_I U_{\bar{\eta}})_{\bar{\eta}} =$$
$$-[\bar{\mu}'_I \dot{F}\Phi]_{\bar{\eta}} + \frac{1}{\sqrt{2u_s}}\ddot{F}[\int_0^{\sqrt{2u_s}\bar{\eta}} U\,d\bar{\eta}' + 2X\int_0^{\sqrt{2u_s}\bar{\eta}} U_X\,d\bar{\eta}'] \tag{4.3.46}$$

46

and

$$2X\dot{F}\Phi_X - F\Phi_{\bar{\eta}} + \frac{1}{\sqrt{2u_s}}T_{I\bar{\eta}}\left[\int_0^{\sqrt{2u_s\bar{\eta}}} U\,d\bar{\eta}' + 2X\int_0^{\sqrt{2u_s\bar{\eta}}} U_X\,d\bar{\eta}'\right] =$$

$$\frac{1}{P_r}[\bar{\mu}_I\Phi_{\bar{\eta}} + \bar{\mu}_I'T_{I\bar{\eta}}\Phi]_{\bar{\eta}}$$

$$+(\gamma-1)M^2[-2\ddot{F}\bar{\mu}_I U_{\bar{\eta}} + \bar{\mu}_I'\ddot{F}^2\Phi] + \frac{2X\beta}{\epsilon\rho}\Omega. \tag{4.3.47}$$

For $\bar{\eta} = O(1)$, the reaction term in equation (4.3.47) is exponentially small and, therefore, negligible to all orders of the perturbation expansion in this zone.

4.4 Matching the Inner and Outer Solution

4.4.1 Momentum Equation

The inner expansion of u is

$$\begin{aligned}
u_{inner} &= u_I + \epsilon u_0 + \epsilon^{\frac{3}{2}} u_1 + \dots \\
&= u_I + \epsilon(A_1\xi) + \epsilon^{\frac{3}{2}}\{+\bar{u}_1(X)\}\xi + \dots. \tag{4.4.48}
\end{aligned}$$

The outer-region expansion with $\bar{\eta} = \epsilon^{\frac{1}{2}}\xi$ and $X = X$ is

$$\begin{aligned}
u_{outer} &= u_I + \epsilon U(X,\bar{\eta}) + \dots \\
&= u_I + \epsilon\{U(X,0) + U_{\bar{\eta}}(X,0)\bar{\eta} + \dots\} \\
&= u_I + \epsilon U(X,0) + \epsilon^{\frac{3}{2}}U_{\bar{\eta}}(X,0)\xi + \dots. \tag{4.4.49}
\end{aligned}$$

The matching of inner and outer expansions of U from equations (4.4.48) and (4.4.49) for each ξ forces $A_1 = 0$ so that

$$U(X,0) = 0 \tag{4.4.50}$$

and

$$U_{\bar{\eta}}(X,0) = \bar{u}_1(X). \tag{4.4.51}$$

47

These are the boundary conditions used to solve the momentum equation for the outer region.

4.4.2 Energy Equation

In the reaction zone, the temperature solution is of the form

$$
\begin{aligned}
T_{inner} &= T_I + \epsilon \Psi_0(X,\xi) + \dots \\
&= T_I + \epsilon\{\bar{\psi}_0(X) + \epsilon^{1/2}\bar{\psi}_1(X,\xi)\} + \dots
\end{aligned}
\tag{4.4.52}
$$

which in the limit $\xi \to \infty$ becomes

$$
T_{inner} = T_I + \epsilon\bar{\psi}_0(X) + \epsilon^{3/2}\{A\xi + B\} + \dots
\tag{4.4.53}
$$

where

$$
A = -\frac{\bar{D}\sqrt{\pi}}{2\sqrt{b^*}}Xe^{\bar{\psi}_0(X)},
\tag{4.4.54}
$$

$$
B = -\frac{\bar{D}}{2b^*}Xe^{\bar{\psi}_0(X)},
\tag{4.4.55}
$$

and

$$
\bar{D} = \frac{2P_r\beta}{\bar{\mu}(T_{ad})}.
\tag{4.4.56}
$$

The expansion for temperature in the outer region is

$$
\begin{aligned}
T_{outer} &= T_I + \epsilon\Phi + \dots \\
&= T_I + \epsilon\{\Phi(X,0) + \Phi_{\bar{\eta}}(X,0)\bar{\eta}\} + \dots.
\end{aligned}
\tag{4.4.57}
$$

Since $\bar{\eta} = \epsilon^{1/2}\xi$, the outer solution becomes

$$
T_{outer} = T_I + \epsilon\Phi(X,0) + \epsilon^{3/2}\Phi_{\bar{\eta}}(X,0)\xi + \dots,
\tag{4.4.58}
$$

and for the inner solution to match with the outer solution for all ξ forces

$$
\Phi(X,0) = \bar{\psi}_0(X)
\tag{4.4.59}
$$

48

and

$$\Phi_{\bar{\eta}}(X, 0) = -\frac{\bar{D}\sqrt{\pi}}{2\sqrt{b^*}} X e^{\bar{\psi}_0(X)}. \tag{4.4.60}$$

These are the boundary conditions used to solve the energy equation for the outer region.

49

Chapter 5

NUMERICAL SOLUTIONS

5.1 Introduction

To solve the perturbed energy and momentum equations in the outer region numerically, it is noticed that the numerical integrations are simplified by using the transformation

$$\rho = \dot{F} = \frac{dF}{d\bar{\eta}}. \tag{5.1.1}$$

Thus, the domain has changed from $0 \leq \bar{\eta} \leq \infty$ to $u_s \geq \rho \geq u_s - 1$. In terms of the spatial variable ρ (note that ρ no longer refers to the density), the inert equations are

$$- F\ddot{F}T_{I\rho} = \frac{1}{P_r}\{\overline{(\bar{\mu}(T_I)\dot{F})}T_{I\rho} + \bar{\mu}(T_I)\ddot{F}^2 T_{I\rho\rho}\} + (\gamma - 1)M^2\bar{\mu}(T_I)\ddot{F}^2 \tag{5.1.2}$$

and

$$F\ddot{F} + (\overline{\bar{\mu}\dot{\ddot{F}}}) = 0. \tag{5.1.3}$$

50

5.2 Energy Equation

The perturbed energy equation (4.3.47) is transformed in terms of the outer variable ρ and is simplified by adding the term

$$- (\overline{\bar{\mu}\ddot{F}})\Phi_\rho \tag{5.2.4}$$

to both sides to get

$$2X\dot{F}\Phi_X + \frac{1}{\sqrt{2u_s}}\ddot{F}T_{I\rho}\{\int_0^{\sqrt{2u_s}\bar{\eta}} Ud\bar{\eta}' + 2X\int_0^{\sqrt{2u_s}\bar{\eta}} U_X d\bar{\eta}'\} =$$

$$(\frac{1}{P_r} - 1)[(\overline{\bar{\mu}\ddot{F}})\Phi_\rho] + \frac{1}{P_r}\bar{\mu}_I(T_I)\ddot{F}^2\Phi_{\rho\rho} + \frac{1}{P_r}[(\overline{\bar{\mu}_I'(T_I)\Phi\dot{\ddot{F}}})T_{I\rho} + \bar{\mu}_I'\Phi\ddot{F}^2 T_{I\rho\rho}]$$

$$+(\gamma - 1)M^2[-2\ddot{F}^2\bar{\mu}_I U_\rho + \bar{\mu}_I'\ddot{F}^2\Phi]. \tag{5.2.5}$$

The reaction term is zero in this outer region. The integrals on the left-hand side of the above equation are still in terms of the variable $\bar{\eta}$. These integrals, in terms of ρ, are

$$\begin{aligned} \bar{I}_1 &= \frac{1}{\sqrt{2u_s}}\int_0^{\sqrt{2u_s}\bar{\eta}} U_X d\bar{\eta}' \\ &= \int_{u_s}^\rho \frac{U_X(\rho',X)}{\ddot{F}(\rho')}d\rho' \end{aligned} \tag{5.2.6}$$

and

$$\begin{aligned} I_2 &= \frac{1}{\sqrt{2u_s}}\int_0^{\sqrt{2u_s}\bar{\eta}} U(\bar{\eta}',X)d\bar{\eta}' \\ &= \int_{u_s}^\rho \frac{U(\rho',X)}{\ddot{F}(\rho')}d\rho'. \end{aligned} \tag{5.2.7}$$

Now the variable

$$\sigma = ln(\hat{A}X) \tag{5.2.8}$$

is used to transform the product $X\partial/\partial X$ to $\partial/\partial\sigma$. $\hat{A}$ is chosen later for convenience. The integral $X\bar{I}_1$ is transformed to new variable σ to get

$$X\bar{I}_1 = \frac{\partial}{\partial\sigma}\int_{u_s}^\rho \frac{U(\rho',X)}{\ddot{F}(\rho')}d\rho' = I_1. \tag{5.2.9}$$

51

The energy equation is now

$$2\dot{F}\Phi_\sigma - \frac{1}{P_r}b\Phi_{\rho\rho} = [(\frac{1}{P_r} - 1)a + \frac{1}{P_r}cT_{I\rho}]\Phi_\rho$$

$$+[\frac{1}{P_r}(bdT_{I\rho} + ae)T_{I\rho} + \frac{1}{P_r}cT_{I\rho\rho} + (\gamma - 1)M^2c]\Phi$$

$$-2(\gamma - 1)M^2bU_\rho - \ddot{F}T_{I\rho}I_2 - 2\dot{F}T_{I\rho}I_1. \qquad (5.2.10)$$

Multiplying equation (5.2.10) by $-P_r/b$ and rearranging the terms, the final form of the energy equation is

$$\Phi_{\rho\rho} - g\Phi_\sigma = \bar{A}\Phi_\rho + \bar{B}\Phi + \bar{C}U_\rho + \bar{D}I_2 + \bar{E}I_1 \qquad (5.2.11)$$

with the coefficients

$$\bar{A} = -\frac{P_r}{b}[\frac{1 - P_r}{P_r}a + \frac{cT_{I\rho}}{P_r}], \qquad (5.2.12)$$

$$\bar{B} = P_r e\frac{F\ddot{F}}{b}T_{I\rho} - d(T_{I\rho})^2, \qquad (5.2.13)$$

$$\bar{C} = 2P_r(\gamma - 1)M^2, \qquad (5.2.14)$$

$$\bar{D} = \frac{P_r\ddot{F}T_{I\rho}}{b}, \qquad (5.2.15)$$

and

$$\bar{E} = \frac{2P_r\ddot{F}T_{I\rho}}{b} \qquad (5.2.16)$$

where

$$a = \overline{\dot{\mu}\ddot{F}}, \qquad (5.2.17)$$

$$b = \bar{\mu}\ddot{F}^2, \qquad (5.2.18)$$

$$c = \bar{\mu}'\ddot{F}^2, \qquad (5.2.19)$$

$$d = (\frac{\bar{\mu}'}{\bar{\mu}})', \qquad (5.2.20)$$

$$e = \frac{\bar{\mu}'}{\bar{\mu}}, \qquad (5.2.21)$$

52

and

$$g = \frac{2P_r \dot{F}}{b}.$$

(5.2.22)

The boundary conditions (4.4.59) and (4.4.60) at $\bar{\eta} = 0$, in terms of the integration variables σ and ρ, are

$$\Phi(\sigma, u_s) = \tilde{\psi}_0(\sigma)$$

(5.2.23)

and

$$\Phi_\rho(\sigma, u_s) = -\frac{P_r \beta \sqrt{\pi}}{\bar{\mu}(T_{ad}) \sqrt{b^*} \ddot{F}(0)} \frac{e^\sigma}{\hat{A}} e^{\tilde{\psi}_0(\sigma)}.$$

(5.2.24)

Now, for convenience, choose

$$\hat{A} = -\frac{P_r \beta \sqrt{\pi}}{\bar{\mu}(T_{ad}) \sqrt{b^*} \ddot{F}(0)},$$

(5.2.25)

and equation (5.2.24) is written as

$$\Phi_\rho(\sigma, u_s) = e^{[\tilde{\psi}_0(\sigma) + \sigma]}$$

(5.2.26)

where

$$\tilde{\psi}_0(\sigma) = \tilde{\psi}_0(X).$$

(5.2.27)

A homogeneous boundary condition is required at $\rho = u_s - 1$.

5.3 Momentum Equation

Using the transformation (5.1.1), the governing equation for velocity U in terms of the computational variable ρ is

$$2X\dot{F}U_X - F\ddot{F}U_\rho - \{\overline{\dot{\bar{\mu}}\dot{F}}U_\rho + \bar{\mu}(T_I)\dot{F}^2 U_{\rho\rho}\} =$$
$$-[I] + \ddot{F} \int_{u_s}^{\rho} \frac{U(\rho', X)}{\dot{F}(\rho')} d\rho' + \ddot{F} \int_{u_s}^{\rho} \frac{U_X(\rho', X)}{\dot{F}(\rho')} d\rho'$$

(5.3.28)

53

with

$$[I] = [\Phi\bar{\mu}'\ddot{F}]_{\bar{\eta}}$$

$$= \Phi_\rho\bar{\mu}'_I\ddot{F}^2 + \Phi\{(\frac{\bar{\mu}'_I}{\bar{\mu}_I})'T_{I\rho}\bar{\mu}_I\ddot{F}^2 + \frac{\bar{\mu}'}{\bar{\mu}}\overline{\dot{\bar{\mu}}_I\ddot{F}}\}. \tag{5.3.29}$$

Using equation (3.2.15) in the left-hand side of equation (5.3.28) and the above relation for I in the right-hand side, the momentum equation simplifies to

$$2X\dot{F}U_X - \bar{\mu}(T_I)\ddot{F}^2U_{\rho\rho} = -\{\bar{\mu}'_I\ddot{F}^2\Phi_\rho + [(\frac{\bar{\mu}'_I}{\bar{\mu}_I})'\bar{\mu}_I\ddot{F}^2T_{I\rho} + \frac{\bar{\mu}'_I}{\bar{\mu}}\overline{\dot{\bar{\mu}}_I\ddot{F}}]\Phi\}$$

$$+ \ddot{F}\int_{u_s}^{\rho}\frac{U(\rho',X)}{\dot{F}(\rho')}d\rho' + 2X\ddot{F}\int_{u_s}^{\rho}\frac{U_X}{\dot{F}(\rho')}d\rho'. \tag{5.3.30}$$

The transformation $\sigma = ln(\hat{A}X)$ produces the equation

$$2\dot{F}U_\sigma - bU_{\rho\rho} = -c\Phi_\rho - [bdT_{I\rho} + ae]\Phi + \ddot{F}I_2 + 2\dot{F}I_1. \tag{5.3.31}$$

Multiplying both sides of this equation by $-1/b$ and rearranging the terms, the momentum equation becomes

$$U_{\rho\rho} - \bar{\bar{g}}U_\sigma = \bar{\bar{A}}\Phi_\rho + \bar{\bar{B}}\Phi + \bar{\bar{D}}I_2 + \bar{\bar{E}}I_1 \tag{5.3.32}$$

where a, b, c, d, e, I_1 and I_2 are the same as before and

$$\bar{\bar{g}} = \frac{2\dot{F}}{b}, \tag{5.3.33}$$

$$\bar{\bar{A}} = \frac{c}{b}, \tag{5.3.34}$$

$$\bar{\bar{B}} = \frac{1}{b}[bdT_{I\rho} + ae], \tag{5.3.35}$$

$$\bar{\bar{D}} = -\frac{\ddot{F}}{b}, \tag{5.3.36}$$

and

$$\bar{\bar{E}} = \frac{-2\dot{F}}{b}. \tag{5.3.37}$$

54

The boundary conditions (4.4.50) and (4.4.51) at $\bar{\eta} = 0$, in terms of the integration variables σ and ρ, are

$$U(\sigma, u_s) = 0 \tag{5.3.38}$$

and

$$U_\rho(\sigma, u_s) = \tilde{u}_1(\sigma). \tag{5.3.39}$$

A homogeneous condition is required at $\rho = u_s - 1$.

5.4 Derivation of the Initial Condition

The solutions of the perturbed energy and momentum equations are numerically determined using a Crank-Nicolson algorithm with finite differencing in the ρ−direction and implicit marching in the σ−direction. Since $\Phi(\sigma, \rho) \to 0$ as $\sigma \to -\infty$, an asymptotic form of the initial condition for energy and momentum is needed to start the Crank-Nicolson algorithm; therefore, let

$$\Phi(\sigma, \rho) = \hat{\psi}_0(\rho)e^\sigma + O(e^{2\sigma}) \tag{5.4.40}$$

and

$$U(\sigma, \rho) = \hat{u}_0(\rho)e^\sigma + O(e^{2\sigma}). \tag{5.4.41}$$

Using these in the energy equation (5.2.11) gives

$$\frac{d^2\hat{\psi}_0}{d\rho^2} - g\hat{\psi}_0 = \bar{A}\frac{d\hat{\psi}_0}{d\rho} + \bar{B}\hat{\psi}_0 + \bar{C}\frac{d\hat{u}_0}{d\rho} + (\bar{D} + \bar{E})I \tag{5.4.42}$$

with the boundary conditions

$$\hat{\psi}_{0\rho}(u_s) = 1 \tag{5.4.43}$$

and

$$\hat{\psi}_0(u_s - 1) = 0. \tag{5.4.44}$$

55

Similarly, using (5.4.40) and (5.4.41) in the momentum equation (5.3.32) gives

$$\frac{d^2\hat{u}_0}{d\rho^2} - \bar{\bar{g}}\hat{u}_0 = \bar{\bar{A}}\frac{d\hat{\psi}_0}{d\rho} + \bar{\bar{B}}\hat{\psi}_0 + (\bar{\bar{D}} + \bar{\bar{E}})I \qquad (5.4.45)$$

with the boundary conditions

$$\hat{u}_0(u_s) = 0 \qquad (5.4.46)$$

and

$$\hat{u}_0(u_s - 1) = 0. \qquad (5.4.47)$$

These differential equations are solved numerically using COLSYS, and the relations (5.4.40) and (5.4.41) give appropriate initial conditions when σ is chosen to be a large negative number.

5.5   System of Equations

The complete system of differential and partial differential equations for the adiabatic wall that is solved numerically is

$$F\ddot{F} + \overline{\dot{\bar{\mu}F}} = 0 \qquad (5.5.48)$$

with boundary conditions

$$F(0) = 0, \qquad (5.5.49)$$

$$\dot{F}(0) = u_s, \qquad (5.5.50)$$

and

$$\dot{F}(\infty) = u_s - 1; \qquad (5.5.51)$$

$$- F\ddot{F}T_{I\rho} = \frac{1}{P_r}\{(\overline{\bar{\mu}(T_I)\dot{F}})T_{I\rho} + \bar{\mu}(T_I)\ddot{F}^2 T_{I\rho\rho}\} + (\gamma - 1)M^2\bar{\mu}(T_I)\ddot{F}^2 \qquad (5.5.52)$$

56

with boundary conditions

$$T_{I\rho}(u_s) = 0 \qquad (5.5.53)$$

and

$$T_I(u_s - 1) = 1; \qquad (5.5.54)$$

$$\Phi_{\rho\rho} - g\Phi_\sigma = \bar{A}\Phi_\rho + \bar{B}\Phi + \bar{C}u_{0\rho} + \bar{D}I_2 + \bar{E}I_1 \qquad (5.5.55)$$

with boundary conditions

$$\Phi(\sigma, u_s) = \tilde{\psi}_0(\sigma), \qquad (5.5.56)$$

$$\Phi_\rho(\sigma, u_s) = e^{\tilde{\psi}_0(\sigma)+\sigma}, \qquad (5.5.57)$$

and

$$\Phi(\sigma, u_s - 1) = 0; \qquad (5.5.58)$$

and

$$U_{\rho\rho} - \bar{\bar{g}}U_\sigma = \bar{\bar{A}}\Phi_\rho + \bar{\bar{B}}\Phi + \bar{\bar{D}}I_2 + \bar{\bar{E}}I_1 \qquad (5.5.59)$$

with boundary conditions

$$U(\sigma, u_s) = 0, \qquad (5.5.60)$$

$$U_\rho(\sigma, u_s) = \tilde{u}_1(\sigma), \qquad (5.5.61)$$

and

$$U(\sigma, u_s - 1) = 0. \qquad (5.5.62)$$

The initial conditions are as derived in the previous section.

57

5.6 Numerical Results and Discussions

The system (5.5.55) through (5.5.62) is overdetermined and, hence, has a solution only for particular values of $\tilde{\psi}_0(\sigma)$ and $\tilde{u}_1(\sigma)$. This system is solved numerically using a Crank-Nicolson algorithm with finite differencing in the ρ-direction and implicit marching in the σ-direction. The starting value of σ is determined to be -10. Values of σ less than -10 give the same output. A value of $\tilde{\psi}_0(\sigma)$ is chosen and the equations (5.5.55) and (5.5.59) are solved subject to (5.5.57), (5.5.58), (5.5.60) and (5.5.62). The secant method is used to update the value of $\tilde{\psi}_0(\sigma)$ that would also satisfy (5.5.56). The function $\tilde{u}_1(\sigma)$ is then directly computed using (5.5.61). The grid size for ρ is 0.001, and a variable grid size is used for the σ-direction starting with 0.01. As σ increases, the perturbed temperature near the wall becomes infinite, signaling thermal runaway. Thus, the step size is reduced to 0.000001 near the ignition distance. Figure 5.1 shows the perturbed temperature at the boundary versus σ for two different values of the Mach number. The dashed curve is for $M = 5$ and the solid curve is for $M = 2$. The point at which $\Phi(\sigma, \rho)$ becomes unbounded is denoted by σ_* and is referred to as the ignition distance. The plot shows that the non-dimensional ignition distance for Mach number $M = 5$ is shorter than for $M = 2$. The perturbed temperature profile at $\sigma = \sigma_*$ as a function of $(u_s - \rho)$ is shown in Figure 5.2. The dashed curve is for Mach number 5.0 and the solid curve is for Mach number 2.0. The graph shows the steady decrease in the perturbed temperature away from the boundary. The temperature values for $M = 5.0$ are higher than the temperature values for $M = 2.0$ at each point. In this formulation, the non-dimensional ignition distance depends mainly on the Mach number, and it is determined that the Prandtl number does not play a significant role in determining the ignition distance. Figure 5.3 is a plot of the ignition distance σ_* versus Mach number. This graph shows that

58

σ_* is nearly a linearly decreasing function of the Mach number. To see the effect of the Mach number on the velocity, the perturbed velocity profile at $\sigma = \sigma_*$ as a function of $(u_s - \rho)$ is shown in Figure 5.4 for Mach numbers $M = 2.0$ and $M = 5.0$. The dashed curve is for $M = 5.0$ and the solid curve is for $M = 2.0$.
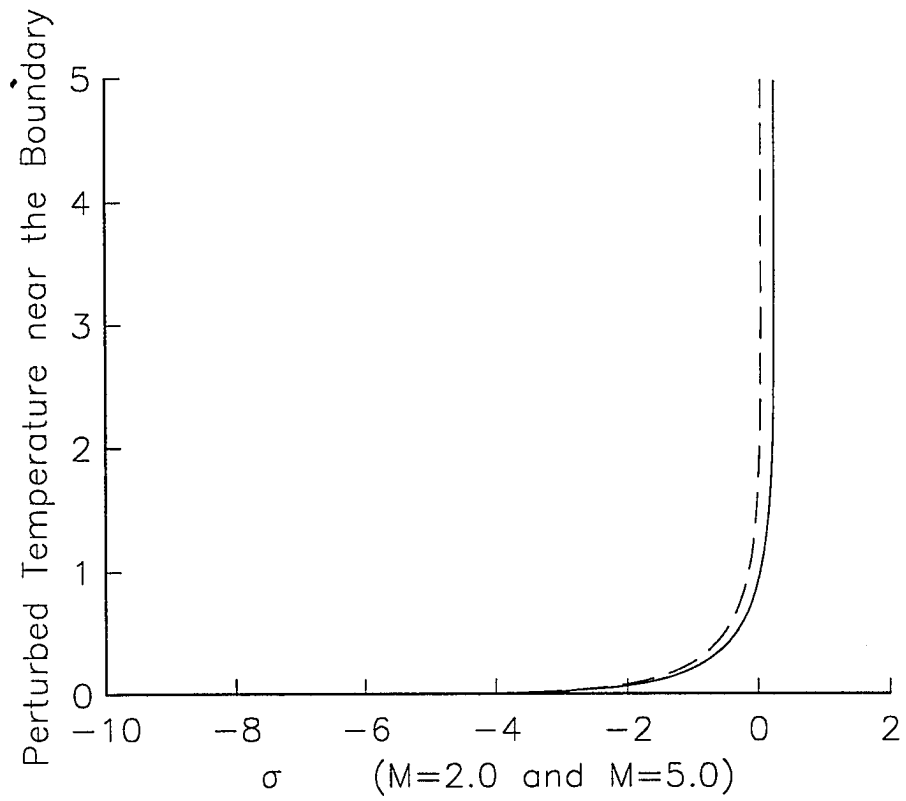
Figure 5.1: Perturbed temperature growth with σ at the ignition point. Solid curve for Mach number $M = 2.0$ and dashed curve for $M = 5.0$.

60
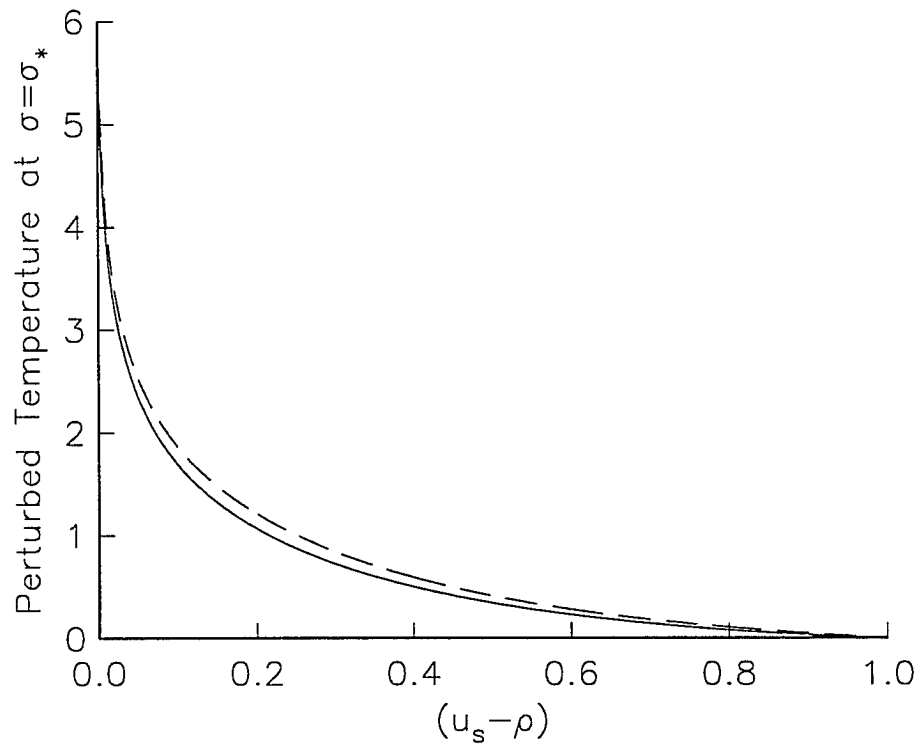
Figure 5.2: Perturbed temperature profile at ignition distance σ_* as a function of $(u_s - \rho)$. Solid curve for $M = 2.0$ and dashed curve for $M = 5.0$.

61
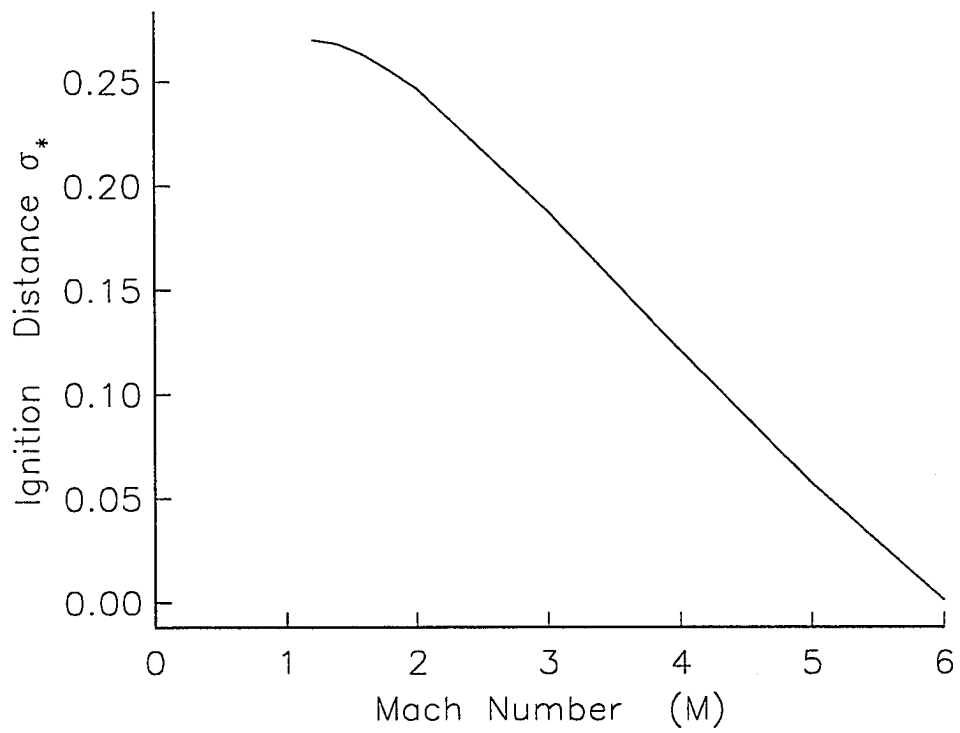
Figure 5.3: Ignition distance σ_* as a function of Mach number M.
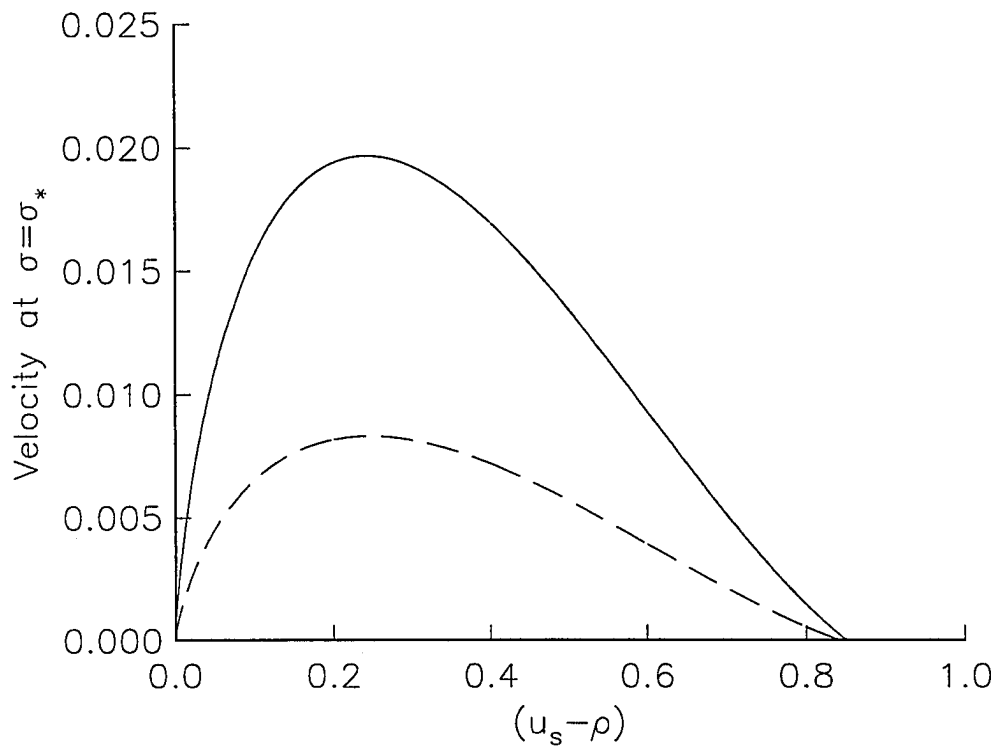
Figure 5.4: The perturbed velocity profile at $\sigma = \sigma_*$ as a function of $(u_s - \rho)$. Solid curve for $M = 2.0$ and dashed curve for $M = 5.0$.

63

Chapter 6

ANALYSIS OF THE

ISOTHERMAL WALL

6.1   Introduction

Now consider the case in which the wall temperature is held constant. The situation where viscous dissipation mainly provides the heating source for temperature increase is analyzed, and it is assumed that the surface temperature T_s is less than the maximum temperature T_{max}. The inert-state temperature profile, Figure 3.7, has a maximum value at $\bar{\eta} = \eta^*$ which lies in the interior of the boundary layer, and since the reaction will initiate near the hottest location in the inert-state flow field, the reaction zone will be in the interior. Therefore, in the isothermal case, the boundary layer consists of two outer regions, $0 < \bar{\eta} < \eta^*$ and $\eta^* < \bar{\eta} < \infty$, separated by an inner, reaction zone near η^*. The exponent of the reaction term suggests that, in the limit $E \to \infty$ being considered, the reaction term will be significant only in the region

64

where $|T - T_{max}| = O(E^{-1})$. Using this fact, the thickness of the inner reaction zone is determined to be $O(\epsilon^{1/2})$.

6.2 Reaction Zone Analysis

To examine the behaviour in the reaction zone for the isothermal wall, the inner stretched variable ξ is introduced as

$$\bar{\eta} = \eta^* + \epsilon^{1/2}\xi. \qquad (6.2.1)$$

Also, as in the adiabatic case, the expansions of the inert temperature, mass fraction, viscosity and streamfunction used in the forthcoming analysis are

$$T_I = T_I(\eta^*) + \epsilon\frac{\ddot{T}_I(\eta^*)}{2}\xi^2 + \ldots, \qquad (6.2.2)$$

$$Y_I = 1, \qquad (6.2.3)$$

$$\bar{\mu} = \bar{\mu}(T_{max}) + \epsilon\frac{1}{2}\bar{\mu}'(T_{max})\ddot{T}_I(\eta^*)\xi^2 + \ldots, \qquad (6.2.4)$$

$$\bar{\mu}' = \bar{\mu}'(T_{max}) + \epsilon\frac{1}{2}\bar{\mu}''(T_{max})\ddot{T}_I(\eta^*)\xi^2 + \ldots, \qquad (6.2.5)$$

$$F = F(\eta^*) + \epsilon^{\frac{1}{2}}\dot{F}(\eta^*)\xi + \ldots, \qquad (6.2.6)$$

$$\dot{F} = \dot{F}(\eta^*) + \epsilon^{\frac{1}{2}}\ddot{F}(\eta^*)\xi + \ldots, \qquad (6.2.7)$$

and

$$\ddot{F} = \ddot{F}(\eta^*) + \epsilon^{\frac{1}{2}}\frac{d^3 F}{d\bar{\eta}^3}(\eta^*)\xi + \ldots \qquad (6.2.8)$$

where T_{max} is the maximum inert temperature at $\eta = \eta^*$. Using the transformation (6.2.1) and expansions (6.2.2) - (6.2.8) in the perturbed momentum and energy equations (4.1.7) and (4.1.8) and keeping only $O(\epsilon^{-1/2})$ and lower-order terms gives

$$- \epsilon^{-1}\bar{\mu}(T_{max})\bar{u}_{0\xi\xi} = \epsilon^{\frac{-1}{2}}\{F(\eta^*)\bar{u}_{0\xi} - \bar{\mu}'(T_{max})\ddot{F}(\eta^*)\Psi_{0\xi}\} \qquad (6.2.9)$$

65

and

$$-\epsilon^{\frac{-1}{2}}F(\eta^*)\Psi_{0\xi} = \epsilon^{-1}\frac{1}{P_r}\bar{\mu}(T_{max})\Psi_{0\xi\xi}$$
$$-2\epsilon^{\frac{-1}{2}}(\gamma-1)M^2\ddot{F}(\eta^*)\bar{\mu}(T_{max})u_{0\xi} + \epsilon^{-1}\frac{2X\beta}{\rho}\Omega \qquad (6.2.10)$$

which are written as

$$\bar{u}_{0\xi\xi} = \epsilon^{1/2}[\frac{\bar{\mu}'(T_{max})}{\bar{\mu}(T_{max})}\ddot{F}(\eta^*)\ddot{\bar{\Psi}}_{0\xi} - \frac{F(\eta^*)}{\bar{\mu}(T_{max})}\bar{u}_{0\xi}] \qquad (6.2.11)$$

and

$$\Psi_{0\xi\xi} = -\frac{2XP_r}{\bar{\mu}(T_{max})}\frac{\beta}{\rho}\Omega - \epsilon^{\frac{1}{2}}\frac{P_rF(\eta^*)}{\bar{\mu}(T_{max})}\Psi_{0\xi} + \epsilon^{1/2}2P_r(\gamma-1)M^2\ddot{F}(\eta^*)\bar{u}_{0\xi}. \qquad (6.2.12)$$

The form of the reaction term under these assumption is

$$\begin{aligned}\Omega &= D\rho Y e^{-E/T}\\ &= D_0\epsilon^\delta \rho Y e^{E(1/T^*-1/T)}\\ &= D_0\epsilon^\delta \rho Y e^{(-\bar{b}\xi^2+\Psi_0)} \qquad (6.2.13)\end{aligned}$$

where $T^* = T_{max}$ and quantities D_0 and δ are chosen in the analysis.
Also,

$$\epsilon = \frac{T_{max}^2}{E} \qquad (6.2.14)$$

and

$$\bar{b} = -\frac{\ddot{T}_I(\eta^*)}{2}. \qquad (6.2.15)$$

Now equation (6.2.12) gives

$$\Psi_{0\xi\xi} = -\epsilon^\delta\frac{2XP_r}{\bar{\mu}(T_{max})}\beta D_0 e^{-\bar{b}\xi^2+\Psi_0}$$
$$-\epsilon^{1/2}\frac{P_rF(\eta^*)}{\bar{\mu}(T_{max})}\Psi_{0\xi} + \epsilon^{1/2}2P_r(\gamma-1)M^2\ddot{F}(\eta^*)\bar{u}_{0\xi}. \qquad (6.2.16)$$

66

Achieving an asymptotic match with the outer solutions requires that $\Psi_0(X,\xi)$ be expressed as

$$\Psi_0(X,\xi) = \bar{\psi}_0(X) + \epsilon^{1/2}\bar{\psi}_1(X,\xi), \tag{6.2.17}$$

and balancing terms in the momentum equation requires that

$$\bar{u}_0(X,\xi) = u_0(X,\xi) + \epsilon^{1/2}u_1(X,\xi). \tag{6.2.18}$$

The governing system is now

$$u_{0\xi\xi} = 0, \tag{6.2.19}$$

$$u_{1\xi\xi} = -\frac{F(\eta^*)}{\bar{\mu}(T_{max})}u_{0\xi}, \tag{6.2.20}$$

and

$$\epsilon^{1/2}\bar{\psi}_{1\xi\xi} = -\epsilon^{\delta}\frac{2XP_r}{\bar{\mu}(T_{max})}\beta D_0 e^{\bar{\psi}_0(X)}e^{-\bar{b}\xi^2} + \epsilon^{1/2}2P_r(\gamma-1)M^2\ddot{F}(\eta^*)u_{0\xi}. \tag{6.2.21}$$

For the reaction term to be included in the analysis, $\delta = 1/2$. By choosing δ, T^* and for convenience $D_0 = 1$, the choice of the length scale for the original problem is complete. The equation is now simply

$$\bar{\psi}_{1\xi\xi} = -\bar{D}Xe^{\bar{\psi}_0(X)}e^{-\bar{b}\xi^2} + 2P_r(\gamma-1)M^2\ddot{F}(\eta^*)u_{0\xi} \tag{6.2.22}$$

where

$$\bar{D} = \frac{2P_r}{\bar{\mu}(T_{max})}\beta. \tag{6.2.23}$$

Integrating equations (6.2.19) and (6.2.20) twice with respect to ξ gives

$$u_0(X,\xi) = A\xi + B \tag{6.2.24}$$

and

$$u_1(X,\xi) = \frac{-F(\eta^*)}{\bar{\mu}(T_{max})}\int_0^\xi u_0(X,\xi')d\xi' + \bar{u}_1(X)\xi \tag{6.2.25}$$

67

where A and B are arbitrary functions of X. It is found later that achieving an asymptotic match with the outer solution requires A to be identically zero. Therefore,

$$u_0(X, \xi) = B \tag{6.2.26}$$

and

$$u_1(X, \xi) = \frac{-F(\eta^*)}{\bar{\mu}(T_{max})} B\xi + \bar{u}_1(X)\xi \tag{6.2.27}$$

where B and $\bar{u}_1(X)$ are determined after matching the inner reaction-zone solution to the outer non-reacting-zone solutions. From equation (6.2.26), $u_{0\xi} \equiv 0$, and the energy equation (6.2.22) reduces to

$$\bar{\psi}_{1\xi\xi} = -\bar{D}Xe^{\bar{\psi}_0(X)}e^{-\bar{b}\xi^2}. \tag{6.2.28}$$

Integrating this equation twice with respect to ξ gives

$$\bar{\psi}_1(X, \xi) = -\bar{D}Xe^{\bar{\psi}_0(X)} \int_0^\xi \int_0^{\xi'} e^{-\bar{b}\xi''^2} d\xi'' d\xi' + \bar{\psi}_{1\xi}(X, \eta^*)\xi. \tag{6.2.29}$$

6.3 Analysis of the Outer Region

Since, in the case of the isothermal wall, the boundary layer is in the interior of the domain at the point η^*, there is an outer region on both sides of η^*. The left-hand side is for $0 < \bar{\eta} < \eta^*$ and the right-hand side is for $\eta^* < \bar{\eta} < \infty$.

6.3.1 Left-Hand-Side Analysis

To analyze the problem in the outer region on the left-hand side, the expansions

$$u(X, \bar{\eta}) = u_I(\bar{\eta}) + \epsilon U(X, \bar{\eta}) + O(\epsilon^2) \tag{6.3.30}$$

and

$$T(X, \bar{\eta}) = T_I(\bar{\eta}) + \epsilon\Phi(X, \bar{\eta}) + O(\epsilon^2) \tag{6.3.31}$$

68

are used in the momentum equation (4.1.1) and the energy equation (4.1.2) to get

$$2X\dot{F}U_X - FU_{\bar{\eta}} - (\bar{\mu}_I U_{\bar{\eta}})_{\bar{\eta}} =$$

$$-[\bar{\mu}_I'\ddot{F}\Phi]_{\bar{\eta}} + \frac{1}{\sqrt{2u_s}}\ddot{F}[\int_0^{\sqrt{2u_s\bar{\eta}}} U\,d\bar{\eta}' + 2X\int_0^{\sqrt{2u_s\bar{\eta}}} U_X\,d\bar{\eta}'] \qquad (6.3.32)$$

and

$$2X\dot{F}\Phi_X - F\Phi_{\bar{\eta}} + \frac{1}{\sqrt{2u_s}}T_{I\bar{\eta}}[\int_0^{\sqrt{2u_s\bar{\eta}}} U\,d\bar{\eta}' + 2X\int_0^{\sqrt{2u_s\bar{\eta}}} U_X\,d\bar{\eta}'] =$$

$$\frac{1}{P_r}[\bar{\mu}_I\Phi_{\bar{\eta}} + \bar{\mu}_I'T_{I\bar{\eta}}\Phi]_{\bar{\eta}}$$

$$+(\gamma - 1)M^2[-2\ddot{F}\bar{\mu}_I U_{\bar{\eta}} + \bar{\mu}_I'\ddot{F}^2\Phi] + \frac{2X\beta}{\epsilon\rho}\Omega. \qquad (6.3.33)$$

6.3.2 Right-Hand-Side Analysis

To analyze the problem in the outer region on the right-hand side, the expansions

$$u(X,\bar{\eta}) = u_I(\bar{\eta}) + \epsilon\bar{U}(X,\bar{\eta}) + O(\epsilon^2) \qquad (6.3.34)$$

and

$$T(X,\bar{\eta}) = T_I(\bar{\eta}) + \epsilon\bar{\Phi}(X,\bar{\eta}) + O(\epsilon^2) \qquad (6.3.35)$$

are used in the momentum equation (4.1.1) and the energy equation (4.1.2) to get the outer-region momentum and energy equations for the right-hand side in terms of variables $\bar{\eta}$ and X. These are

$$2X\dot{F}\bar{U}_X - F\bar{U}_{\bar{\eta}} - (\bar{\mu}_I\bar{U}_{\bar{\eta}})_{\bar{\eta}} =$$

$$-[\bar{\mu}_I'\ddot{F}\bar{\Phi}]_{\bar{\eta}} + \frac{1}{\sqrt{2u_s}}\ddot{F}[\int_0^{\sqrt{2u_s}\eta^*} \bar{U}\,d\bar{\eta}' + \int_{\sqrt{2u_s}\eta^*}^{\sqrt{2u_s\bar{\eta}}} \bar{U}\,d\bar{\eta}'$$

$$+2X\{\int_0^{\sqrt{2u_s}\eta^*} \bar{U}_X\,d\bar{\eta}' + \int_{\sqrt{2u_s}\eta^*}^{\sqrt{2u_s\bar{\eta}}} \bar{U}_X\,d\bar{\eta}'\}] \qquad (6.3.36)$$

and

$$2X\dot{F}\bar{\Phi}_X - F\bar{\Phi}_{\bar{\eta}} + \frac{1}{\sqrt{2u_s}}T_{I\bar{\eta}}[\int_0^{\sqrt{2u_s}\eta^*} \bar{U}\,d\bar{\eta}' + \int_{\sqrt{2u_s}\eta^*}^{\sqrt{2u_s\bar{\eta}}} \bar{U}\,d\bar{\eta}'$$

69

$$+2X\{\int_0^{\sqrt{2u_s}\eta^*} \bar{U}_X\,d\bar{\eta}' + \int_{\sqrt{2u_s}\eta^*}^{\sqrt{2u_s}\bar{\eta}} \bar{U}_X\,d\bar{\eta}'\}] =$$

$$\frac{1}{P_r}[\bar{\mu}_I\bar{\Phi}_{\bar{\eta}} + \bar{\mu}_I'T_{I\bar{\eta}}\bar{\Phi}]_{\bar{\eta}}$$

$$+(\gamma-1)M^2[-2\ddot{F}\bar{\mu}_I\bar{U}_{\bar{\eta}} + \bar{\mu}_I'\ddot{F}^2\bar{\Phi}] + \frac{2X\beta}{\epsilon\rho}\Omega. \qquad (6.3.37)$$

6.4 Matching the Inner and Outer Solutions

6.4.1 Left-Hand-Side Matching—Momentum Equation

The inner-region expansion of u is

$$
\begin{aligned}
u_{inner} &= u_I + \epsilon u_0 + \epsilon^{\frac{3}{2}}u_1 + \ldots \\
&= u_I + \epsilon(A\xi + B) + \epsilon^{\frac{3}{2}}[\frac{-F(\eta^*)}{\bar{\mu}(T_{max})}B + \bar{u}_1(X)]\xi + \ldots. \qquad (6.4.38)
\end{aligned}
$$

The outer-region expansion of u with $\bar{\eta} = \eta^* + \epsilon^{\frac{1}{2}}\xi$ and $X = X$ is

$$
\begin{aligned}
u_{outer} &= u_I + \epsilon U(X,\bar{\eta}) + \ldots \\
&= u_I + \epsilon[U(X,\eta^*) + \epsilon^{\frac{1}{2}}\xi U_{\bar{\eta}}(X,\eta^*)] + \ldots \\
&= u_I + \epsilon U(X,\eta^*) + \epsilon^{\frac{3}{2}}\xi U_{\bar{\eta}}(X,\eta^*) + \ldots. \qquad (6.4.39)
\end{aligned}
$$

The matching of the inner and outer expansions of u for each ξ requires

$$A = 0, \qquad (6.4.40)$$

$$U(X,\eta^*) = B, \qquad (6.4.41)$$

and

$$U_{\bar{\eta}}(X,\eta^*) = \frac{-F(\eta^*)}{\bar{\mu}(T_{max})}B + \bar{u}_1(X). \qquad (6.4.42)$$

These are the boundary conditions at $\bar{\eta} = \eta^*$ used to solve the momentum equation for the left-hand-side outer region. A homogeneous boundary condition is required at $\bar{\eta} = 0$.

70

6.4.2 Left-Hand-Side Matching—Energy Equation

In the reaction zone, the temperature solution is of the form

$$T_{inner} = T_I + \epsilon \Psi_0(X,\xi) + \ldots \tag{6.4.43}$$

$$= T_I + \epsilon \bar{\psi}_0(X) + \epsilon^{\frac{3}{2}} \bar{\psi}_1(X,\xi) + \ldots \tag{6.4.44}$$

The integral in the expression for $\bar{\psi}_1(X,\xi)$ in equation (6.2.29) for the left-hand-side matching as $\xi \to -\infty$ goes as

$$I = \int_0^\xi \int_0^{\xi'} e^{-\bar{b}\xi''^2} d\xi'' d\xi' \quad \to \quad \frac{-\sqrt{\pi}}{2\sqrt{\bar{b}}}\xi + \frac{1}{2\bar{b}} + \ldots \tag{6.4.45}$$

Using this, equation (6.2.29) is written as

$$\bar{\psi}_1(X,\xi) \approx -\bar{D}Xe^{\bar{\psi}_0(X)}[\frac{-\sqrt{\pi}}{2\sqrt{\bar{b}}}\xi + \frac{1}{2\bar{b}}] + \bar{\psi}_{1\xi}(X,\eta^*)\xi \tag{6.4.46}$$

or

$$\bar{\psi}_1(X,\xi) \approx M(X)\xi + N(X) \tag{6.4.47}$$

where

$$M(X) = \frac{\bar{D}X\sqrt{\pi}}{2\sqrt{\bar{b}}}e^{\bar{\psi}_0(X)} + \bar{\psi}_{1\xi}(X,\eta^*) \tag{6.4.48}$$

and

$$N(X) = -\frac{\bar{D}X}{2\bar{b}}e^{\bar{\psi}_0(X)}. \tag{6.4.49}$$

The expression for T_{inner} is therefore

$$T_{inner} = T_I + \epsilon\bar{\psi}_0(X) + \epsilon^{\frac{3}{2}}\{M(X)\xi + N(X)\} + \ldots \tag{6.4.50}$$

The expansion of the temperature on the left-hand side of the outer region is

$$T_{outer} = T_I + \epsilon\Phi(X,\bar{\eta}) + \ldots$$

$$= T_I + \epsilon\{\Phi(X,\eta^*) + \Phi_{\bar{\eta}}(X,\eta^*)(\bar{\eta} - \eta^*) + \ldots\}, \tag{6.4.51}$$

71

and since $\bar{\eta} = \eta^* + \epsilon^{\frac{1}{2}}\xi$,

$$T_{outer} = T_I + \epsilon\Phi(X,\eta^*) + \epsilon^{\frac{3}{2}}\Phi_{\bar{\eta}}(X,\eta^*)\xi + \dots. \qquad (6.4.52)$$

The inner solution matches with the outer solution for each value of ξ if

$$\Phi(X,\eta^*) = \bar{\psi}_0(X) \qquad (6.4.53)$$

and

$$\Phi_{\bar{\eta}}(X,\eta^*) = \frac{\bar{D}X\sqrt{\pi}}{2\sqrt{b}}e^{\bar{\psi}_0(X)} + \bar{\psi}_{1\xi}(X,\eta^*). \qquad (6.4.54)$$

These are the boundary conditions at $\bar{\eta} = \eta^*$ used to solve the energy equation for the left-hand-side outer region. A homogeneous boundary condition is required at $\bar{\eta} = 0$.

6.4.3   Right-Hand-Side Matching—Momentum Equation

The inner-region expansion of u for the right-hand side is

$$
\begin{aligned}
u_{inner} &= u_I + \epsilon u_0 + \epsilon^{\frac{3}{2}}u_1 + \dots \\
&= u_I + \epsilon B + \epsilon^{\frac{3}{2}}[\frac{-F(\eta^*)}{\bar{\mu}(T_{max})}B + \bar{u}_1(X)]\xi + \dots,
\end{aligned}
\qquad (6.4.55)
$$

and outer-region expansion for u with $\bar{\eta} = \eta^* + \epsilon^{\frac{1}{2}}\xi$ and $X = X$ is

$$
\begin{aligned}
u_{outer} &= u_I + \epsilon\bar{U}(X,\bar{\eta}) + \dots \\
&= u_I + \epsilon[\bar{U}(X,\eta^*) + \epsilon^{\frac{1}{2}}\xi\bar{U}_{\bar{\eta}}(X,\eta^*)] + \dots \\
&= u_I + \epsilon\bar{U}(X,\eta^*) + \epsilon^{\frac{3}{2}}\bar{U}_{\bar{\eta}}(X,\eta^*)\xi + \dots.
\end{aligned}
\qquad (6.4.56)
$$

The matching of the inner and outer expansions of u for each ξ requires

$$\bar{U}(X,\eta^*) = B \qquad (6.4.57)$$

72

and

$$\bar{U}_{\bar{\eta}}(X, \rho^*) = \frac{-F(\eta^*)}{\bar{\mu}(T_{max})}B + \bar{u}_1(X). \tag{6.4.58}$$

These are the boundary conditions at $\bar{\eta} = \eta^*$ used to solve the momentum equation for the right-hand-side outer region. A homogeneous boundary condition is required at $\bar{\eta} \to \infty$.

6.4.4 Right-Hand-Side Matching—Energy Equation

For the right-hand side-matching, the integral on the right-hand side of equation (6.2.29) as $\xi \to \infty$ goes as

$$I = \int_0^\xi \int_0^{\xi'} e^{-\bar{b}\xi''^2} d\xi'' d\xi' \quad \to \quad \frac{\sqrt{\pi}}{2\sqrt{\bar{b}}}\xi + \frac{1}{2\bar{b}} + \dots. \tag{6.4.59}$$

Using this, equation (6.2.29) is written as

$$\bar{\psi}_1(X, \xi) \approx -\bar{D}Xe^{\bar{\psi}_0(X)}[\frac{\sqrt{\pi}}{2\sqrt{\bar{b}}}\xi + \frac{1}{2\bar{b}}] + \bar{\psi}_{1\xi}(X, \eta^*)\xi \tag{6.4.60}$$

or

$$\bar{\psi}_1(X, \xi) \approx \bar{M}(X)\xi + \bar{N}(X) \tag{6.4.61}$$

where

$$\bar{M}(X) = \frac{-\bar{D}X\sqrt{\pi}}{2\sqrt{\bar{b}}}e^{\bar{\psi}_0(X)} + \bar{\psi}_{1\xi}(X, \eta^*) \tag{6.4.62}$$

and

$$\bar{N}(X) = -\frac{\bar{D}X}{2\bar{b}}e^{\bar{\psi}_0(X)}. \tag{6.4.63}$$

The inner-region expansion for the temperature T on the right-hand side is

$$\begin{aligned}
T_{inner} &= T_I + \epsilon\bar{\psi}_0(X) + \epsilon^{\frac{3}{2}}\bar{\psi}_1(X, \xi) + \dots \\
&= T_I + \epsilon\bar{\psi}_0(X) + \epsilon^{\frac{3}{2}}\{\bar{M}(X)\xi + \bar{N}(X)\} + \dots,
\end{aligned} \tag{6.4.64}$$

73

and the outer-region expansion with $\bar{\eta} = \eta^* + \epsilon^{\frac{1}{2}}\xi$ and $X = X$ is

$$
\begin{aligned}
T_{outer} &= T_I + \epsilon\bar{\bar{\Phi}}(X,\bar{\eta}) + \ldots \\
&= T_I + \epsilon\{\bar{\bar{\Phi}}(X,\eta^*) + \bar{\bar{\Phi}}_{\bar{\eta}}(X,\eta^*)(\bar{\eta} - \eta^*) + \ldots\} \\
&= T_I + \epsilon\bar{\bar{\Phi}}(X,\eta^*) + \epsilon^{\frac{3}{2}}\bar{\bar{\Phi}}_{\bar{\eta}}(X,\eta^*)\xi + \ldots .
\end{aligned}
\tag{6.4.65}
$$

For the inner expansion to match with the outer expansion for each ξ requires

$$
\bar{\bar{\Phi}}(X,\eta^*) = \bar{\psi}_0(X)
\tag{6.4.66}
$$

and

$$
\bar{\bar{\Phi}}_{\bar{\eta}}(X,\eta^*) = -\frac{\bar{D}X\sqrt{\pi}}{2\sqrt{\bar{b}}}e^{\bar{\psi}_0(X)} + \bar{\psi}_{1\xi}(X,\eta^*)
\tag{6.4.67}
$$

where

$$
\bar{D} = \frac{2P_r\beta}{\bar{\mu}(T_{max})}.
\tag{6.4.68}
$$

These are the boundary conditions at $\bar{\eta} = \eta^*$ to solve the energy equation for the right-hand-side outer region. A homogeneous condition is required at $\bar{\eta} \to \infty$.

74

Chapter 7

NUMERICAL SOLUTIONS

7.1 Introduction

To solve the perturbed momentum and energy equations for the outer region numerically, the integration variables ρ and σ are introduced through the transformations

$$\rho = \frac{dF}{d\bar{\eta}} \tag{7.1.1}$$

and

$$\sigma = \ln(\hat{A}X). \tag{7.1.2}$$

The momentum and energy equations, along with the corresponding boundary conditions for the outer region, are then transformed in terms of the variables ρ and σ. The outer-region problem is now solved for the left-hand-side region $u_s \geq \rho \geq \dot{F}(\eta^*)$ and the right-hand-side region $\dot{F}(\eta^*) \geq \rho \geq u_s - 1$.

7.2 Left-Hand-Side Problem

Proceeding as in the adiabatic case, the simplified momentum and energy equations for the left-hand-side outer region in terms of the integration variables ρ and σ, are

Momentum Equation

$$U_{\rho\rho} - \bar{\bar{g}}U_\sigma = \bar{\bar{A}}\Phi_\rho + \bar{\bar{B}}\Phi + \bar{\bar{D}}I_2 + \bar{\bar{E}}I_1 \qquad (7.2.3)$$

and

Energy Equation

$$\Phi_{\rho\rho} - g\Phi_\sigma = \bar{A}\Phi_\rho + \bar{B}\Phi + \bar{C}U_\rho + \bar{D}I_2 + \bar{E}I_1. \qquad (7.2.4)$$

The boundary condition for the momentum equation at $\bar{\eta} = \eta^*$, as found through matching the inner and outer solution, is

$$U_{\bar{\eta}}(X, \eta^*) = -\frac{F(\eta^*)}{\bar{\mu}(T_{max})}B + \bar{u}_1(X) \qquad (7.2.5)$$

which, in terms of variables ρ and σ, is

$$U_\rho(\sigma, \rho^*) = -\frac{F(\eta^*)}{\bar{\mu}(T_{max})\ddot{F}(\eta^*)}B(\sigma) + \tilde{u}_1(\sigma) \qquad (7.2.6)$$

where

$$B(\sigma) = U(\sigma, \rho^*), \qquad (7.2.7)$$

and

$$\rho^* = \dot{F}(\eta^*). \qquad (7.2.8)$$

The boundary condition at $\rho = u_s$ is

$$U(\sigma, u_s) = 0. \qquad (7.2.9)$$

76

Similarly, the boundary condition for the energy equation at $\bar{\eta} = \eta^*$, as found through matching the inner and outer solution, is

$$\Phi_{\bar{\eta}}(X, \eta^*) = \frac{P_r \beta \sqrt{\pi}}{\bar{\mu}(T_{max})\sqrt{b}} X e^{\bar{\psi}_0(X)} + \bar{\psi}_{1\xi}(X, \eta^*) \qquad (7.2.10)$$

which, in terms of ρ and σ, is

$$\Phi_\rho(\sigma, \rho^*) = \frac{P_r \beta \sqrt{\pi}}{\bar{\mu}(T_{max})\sqrt{b}\ddot{F}(\eta^*)} \frac{e^\sigma}{\hat{A}} e^{\bar{\psi}_0(\sigma)} + \tilde{\psi}_1(\sigma, \rho^*). \qquad (7.2.11)$$

For simplicity, $\hat{A}$ is chosen to be

$$\hat{A} = -\frac{P_r \beta \sqrt{\pi}}{\bar{\mu}(T_{max})\sqrt{b}\ddot{F}(\eta^*)} \qquad (7.2.12)$$

which simplifies (7.2.11) as

$$\Phi_\rho(\sigma, \rho^*) = -e^{[\bar{\psi}_0(\sigma)+\sigma]} + \tilde{\psi}_1(\sigma, \rho^*) \qquad (7.2.13)$$

where

$$\tilde{\psi}_0(\sigma) = \Phi(\sigma, \rho^*) \qquad (7.2.14)$$

and

$$\tilde{\psi}_1(\sigma, \rho^*) = \frac{\bar{\psi}_{1\xi}(X, \eta^*)}{\ddot{F}(\eta^*)}. \qquad (7.2.15)$$

The boundary condition at $\rho = u_s$ is

$$\Phi(\sigma, u_s) = 0. \qquad (7.2.16)$$

7.3   Right-Hand-Side Problem

The simplified momentum and energy equations for the right-hand-side outer region $\dot{F}(\eta^*) \geq \rho \geq u_s - 1$, in terms of the integration variables ρ and σ, are

Momentum Equation

77

$$\bar{U}_{\rho\rho} - \bar{\bar{g}}\bar{U}_\sigma = \bar{\bar{A}}\bar{\Phi}_\rho + \bar{\bar{B}}\bar{\Phi} + \bar{\bar{D}}I_2 + \bar{\bar{E}}I_1 \qquad (7.3.17)$$

and

Energy Equation

$$\bar{\bar{\Phi}}_{\rho\rho} - g\bar{\bar{\Phi}}_\sigma = \bar{A}\bar{\Phi}_\rho + \bar{B}\bar{\Phi} + \bar{C}U_\rho + \bar{D}I_2 + \bar{E}I_1. \qquad (7.3.18)$$

The boundary conditions for the momentum equation, in terms of σ and ρ, are

$$\bar{U}_\rho(\sigma,\rho^*) = -\frac{F(\eta^*)}{\bar{\mu}(T_{max})\ddot{F}(\eta^*)}B(\sigma) + \tilde{u}_1(\sigma) \qquad (7.3.19)$$

and

$$\bar{U}(\sigma, u_s - 1) = 0. \qquad (7.3.20)$$

The boundary conditions for the energy equation, in terms of the variables ρ and σ, are

$$\bar{\bar{\Phi}}_\rho(\sigma,\rho^*) = e^{[\tilde{\psi}_0(\sigma)+\sigma]} + \tilde{\psi}_1(\sigma,\rho^*) \qquad (7.3.21)$$

and

$$\bar{\bar{\Phi}}(\sigma, u_s - 1) = 0. \qquad (7.3.22)$$

Note, that although the temperature has a jump in the derivative from the left-hand side to the right-hand side owing to the heat produced in the reaction term, the momentum equation does not have a jump in the derivative, and thus, the right-hand sides of (7.2.6) and (7.3.19) can be taken as a single unknown function of σ.

7.4 Derivation of the Initial Condition

Proceeding as in the adiabatic case, let $\Phi(\sigma,\rho) = \tilde{\psi}_0(\rho)e^\sigma$ and $U(\sigma,\rho) = \bar{u}_0(\rho)e^\sigma$. The system of differential equations derived and solved numerically for the initial condition needed to start the solution in the outer region is

78

Momentum Equation

$$\frac{d^2\bar{u}_0}{d\rho^2} - \bar{\bar{g}}\bar{u}_0 = \bar{\bar{A}}\frac{d\bar{\psi}_0}{d\rho} + \bar{\bar{B}}\bar{\psi}_0 + (\bar{\bar{D}} + \bar{\bar{E}})I \tag{7.4.23}$$

and

Energy Equation

$$\frac{d^2\bar{\psi}_0}{d\rho^2} - g\bar{\psi}_0 = \bar{A}\frac{d\bar{\psi}_0}{d\rho} + \bar{B}\bar{\psi}_0 + \bar{C}\frac{d\bar{u}_0}{d\rho} + (\bar{D} + \bar{E})I \tag{7.4.24}$$

where

$$I = \int_{u_s}^{\rho} \frac{\bar{u}_0}{\ddot{F}(\rho')} d\rho', \tag{7.4.25}$$

and the boundary conditions are:

Left-Hand Side

$$\bar{u}_0(u_s) = 0, \tag{7.4.26}$$

$$\bar{u}_{0\rho}(\rho^*) = \bar{\bar{g}}_0, \tag{7.4.27}$$

$$\bar{\psi}_0(u_s) = 0, \tag{7.4.28}$$

and

$$\bar{\psi}_{0\rho}(\rho^*) = -1; \tag{7.4.29}$$

Right-Hand Side

$$\bar{u}_{0\rho}(\rho^*) = \bar{\bar{g}}_0, \tag{7.4.30}$$

$$\bar{u}_0(u_s - 1) = 0, \tag{7.4.31}$$

$$\bar{\psi}_{0\rho}(\rho^*) = 1, \tag{7.4.32}$$

and

$$\bar{\psi}_0(u_s - 1) = 0. \tag{7.4.33}$$

79

The unknown constant $\bar{g}_0$ is determined numerically by requiring $\bar{u}_0(\rho^*)$ from the left-hand-side solution to be equal to $\bar{u}_0(\rho^*)$ from the right-hand-side solution.

7.5 System of Equations

The complete system of differential and partial differential equations for the isothermal wall that is solved numerically is

$$F\ddot{F} + \overline{\dot{\bar{\mu}}\ddot{F}} = 0 \qquad (7.5.34)$$

with boundary conditions

$$F(0) = 0, \qquad (7.5.35)$$

$$\dot{F}(0) = u_s, \qquad (7.5.36)$$

and

$$\dot{F}(\infty) = u_s - 1; \qquad (7.5.37)$$

$$- F\ddot{F}T_{I\rho} = \frac{1}{P_r}\{\overline{(\bar{\mu}(T_I)\dot{F})}T_{I\rho} + \bar{\mu}(T_I)\ddot{F}^2 T_{I\rho\rho}\} + (\gamma - 1)M^2\bar{\mu}(T_I)\ddot{F}^2 \qquad (7.5.38)$$

with boundary conditions

$$T_I(u_s) = T_s \qquad (7.5.39)$$

and

$$T_I(u_s - 1) = 1; \qquad (7.5.40)$$

$$\Phi_{\rho\rho} - g\Phi_\sigma = \bar{A}\Phi_\rho + \bar{B}\Phi + \bar{C}U_\rho + \bar{D}I_2 + \bar{E}I_1 \qquad (7.5.41)$$

with boundary conditions

$$\Phi(\sigma, u_s) = 0, \qquad (7.5.42)$$

80

$$\Phi_\rho(\sigma, \rho^*) = -e^{\tilde{\psi}_0(\sigma)+\sigma} + \tilde{\psi}_1(\sigma, \rho^*), \qquad (7.5.43)$$

and

$$\Phi(\sigma, \rho^*) = \tilde{\psi}_0(\sigma); \qquad (7.5.44)$$

$$U_{\rho\rho} - \bar{\bar{g}}U_\sigma = \bar{\bar{A}}\Phi_\rho + \bar{\bar{B}}\Phi + \bar{\bar{D}}I_2 + \bar{\bar{E}}I_1 \qquad (7.5.45)$$

with boundary conditions

$$U(\sigma, u_s) = 0, \qquad (7.5.46)$$

$$U_\rho(\sigma, \rho^*) = \frac{-F(\eta^*)}{\bar{\mu}(T_{max})\ddot{F}(\eta^*)}B(\sigma) + \tilde{u}_1(\sigma), \qquad (7.5.47)$$

and

$$U(\sigma, \rho^*) = B(\sigma); \qquad (7.5.48)$$

$$\bar{\Phi}_{\rho\rho} - g\bar{\Phi}_\sigma = \bar{A}\bar{\Phi}_\rho + \bar{B}\bar{\Phi} + \bar{C}U_\rho + \bar{D}I_2 + \bar{E}I_1 \qquad (7.5.49)$$

with boundary conditions

$$\bar{\Phi}_\rho(\sigma, \rho^*) = e^{[\tilde{\psi}_0(\sigma)+\sigma]} + \tilde{\psi}_1(\sigma, \rho^*), \qquad (7.5.50)$$

$$\bar{\Phi}(\sigma, u_s - 1)) = 0, \qquad (7.5.51)$$

and

$$\bar{\Phi}(\sigma, \rho^*) = \Phi(\sigma, \rho^*); \qquad (7.5.52)$$

and

$$\bar{U}_{\rho\rho} - \bar{\bar{g}}\bar{U}_\sigma = \bar{\bar{A}}\bar{\Phi}_\rho + \bar{\bar{B}}\bar{\Phi} + \bar{\bar{D}}I_2 + \bar{\bar{E}}I_1 \qquad (7.5.53)$$

with boundary conditions

$$\bar{U}_\rho(\sigma, \rho^*) = \frac{-F(\eta^*)}{\bar{\mu}(T_{max})\ddot{F}(\eta^*)}B(\sigma) + \tilde{u}_1(\sigma), \qquad (7.5.54)$$

81

$$\bar{U}(\sigma, u_s - 1) = 0, \qquad (7.5.55)$$

and

$$\bar{U}(\sigma, \rho^*) = U(\sigma, \rho^*). \qquad (7.5.56)$$

The initial conditions are as derived in the previous section.

7.6 Numerical Results and Discussions

The solution to the system (7.5.41) through (7.5.56) is numerically determined using the Crank-Nicolson algorithm with finite differencing in the ρ-direction and implicit marching in the σ-direction. The conditions $\bar{\Phi}(\sigma, \rho^*) = \Phi(\sigma, \rho^*)$ and $\bar{U}(\sigma, \rho^*) = U(\sigma, \rho^*)$ are used along with the secant method to determine the unknowns $\tilde{\psi}_1(\sigma, \rho^*)$ and $\tilde{u}_1(\sigma)$ at each value of σ. As in the adiabatic case, the differential equations are overdetermined; therefore, solutions exist only for certain values of $\tilde{\psi}_1(\sigma, \rho^*)$ and $\tilde{u}_1(\sigma)$. The grid size for ρ is 0.001, and a variable grid size is used for the $\sigma-$direction starting with 0.01. A suitable initial value for σ is found to be -6. The coefficients of the energy and momentum equations depend on the inert-state solutions and physical parameters. The differential equations of the inert-state problem are solved using COLSYS. It is observed that as σ increases, the perturbed temperature at ρ^* becomes infinite, signaling thermal runaway, thus, the step size is reduced to 0.000001 as σ approaches the ignition distance. This value of σ is denoted by σ_* and is referred to as ignition distance, whereas ρ^* is called the ignition point. The system is solved for different values of the physical parameters, and the effects of these parameters on ignition distance and ignition point are analyzed. For Mach number $M = 5.0$ and surface temperature $T_s = 1.0$, the increase of temperature with σ at ignition point ρ^* is shown in Figure 7.1. Thermal runaway is found at ignition distance $\sigma_* = 0.4287$. The

82

above system is also solved for fixed Mach number $M = 2.5$ and different values for surface temperature T_s ranging from 0.5 through 1.8. The temperature at ignition distance σ_* is plotted as a function of $(u_s - \rho)$ in Figure 7.2. The plots show the rapid increase in the temperature in the vicinity of ignition point $(u_s - \rho^*)$ for both the left-hand-side and the right-hand-side solutions. Figure 7.3 is a similar plot for Mach number $M = 5.0$ and surface temperature $T_s = 1.0$. It is determined that in the isothermal wall case the surface temperature T_s has a significant effect on the ignition distance σ_* and the ignition point ρ^*. Figure 7.4 is a plot of the ignition distance σ_* versus the surface temperature T_s for fixed Mach number $M = 2.5$ and Prandtl number $P_r = 1$. The plot shows the decrease in the non-dimensional ignition distance as the surface temperature T_s increases from 0.4 to about 1.2. For $T_s > 1.2$, the value of the non-dimensional ignition distance starts to increase with T_s. Figure 7.5 is a plot of the ignition point $(u_s - \rho^*)$ versus the surface temperature that shows a linear decrease in the ignition point with T_s. Figure 7.6 is a plot of the ignition distance σ_* versus the Mach number M for fixed surface temperature T_s showing the ignition distance decreasing linearly as the Mach number increases. It is determined that the effect of the Mach number M on the ignition point $(u_s - \rho^*)$ is not very significant.
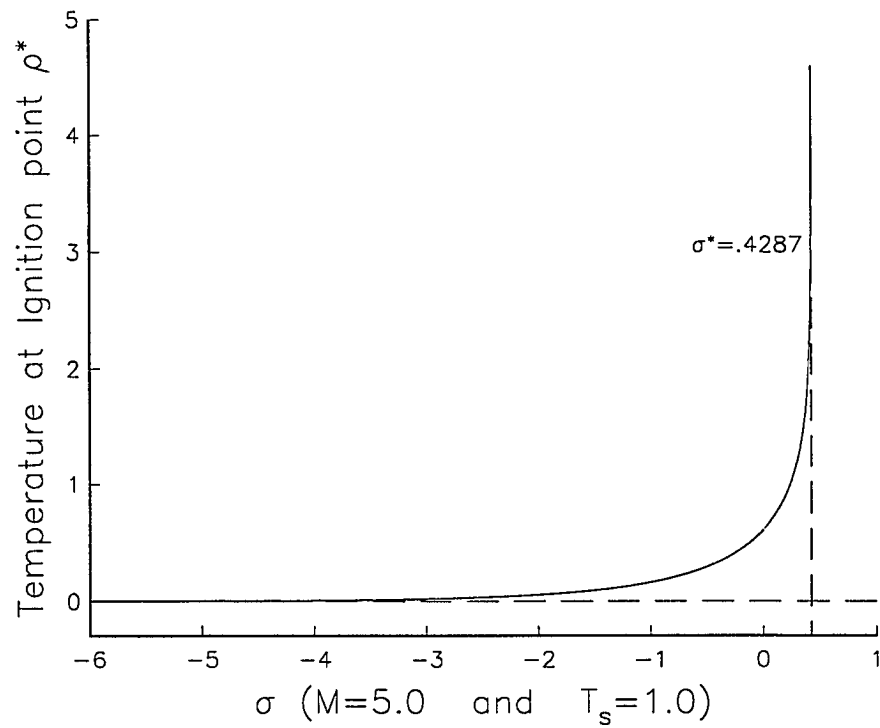
Figure 7.1: Perturbed temperature at ignition point ρ^* as a function of σ for fixed Mach number $M = 5.0$ and surface temperature $T_s = 1.0$.

84
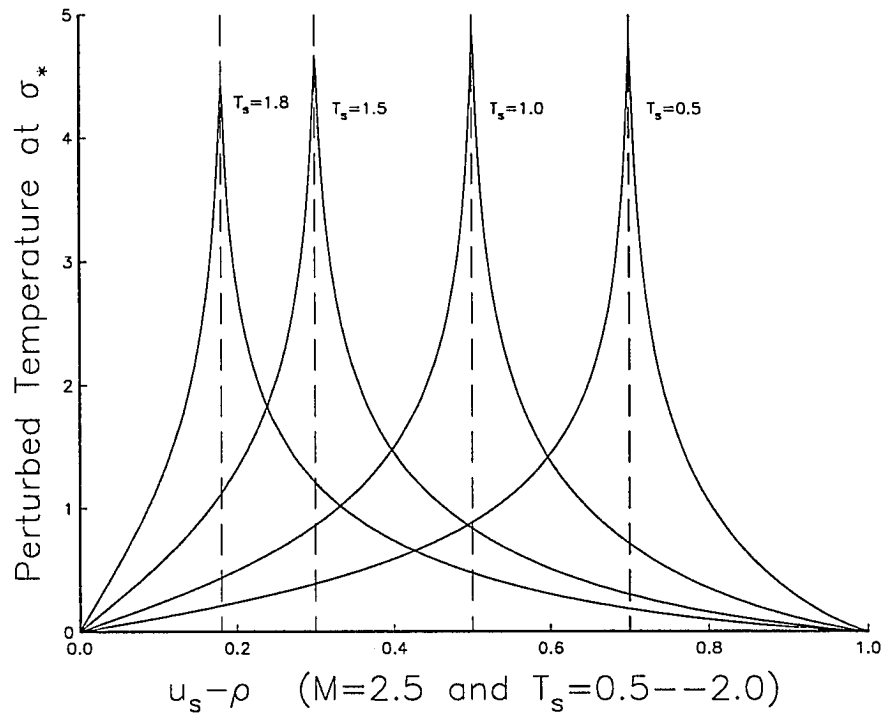
Figure 7.2: Perturbed temperature profiles at ignition distance σ_* as a function of $(u_s - \rho)$ for fixed Mach number $M = 2.5$ and surface temperature $T_s = 0.5$, 1.0, 1.5 and 1.8.

85
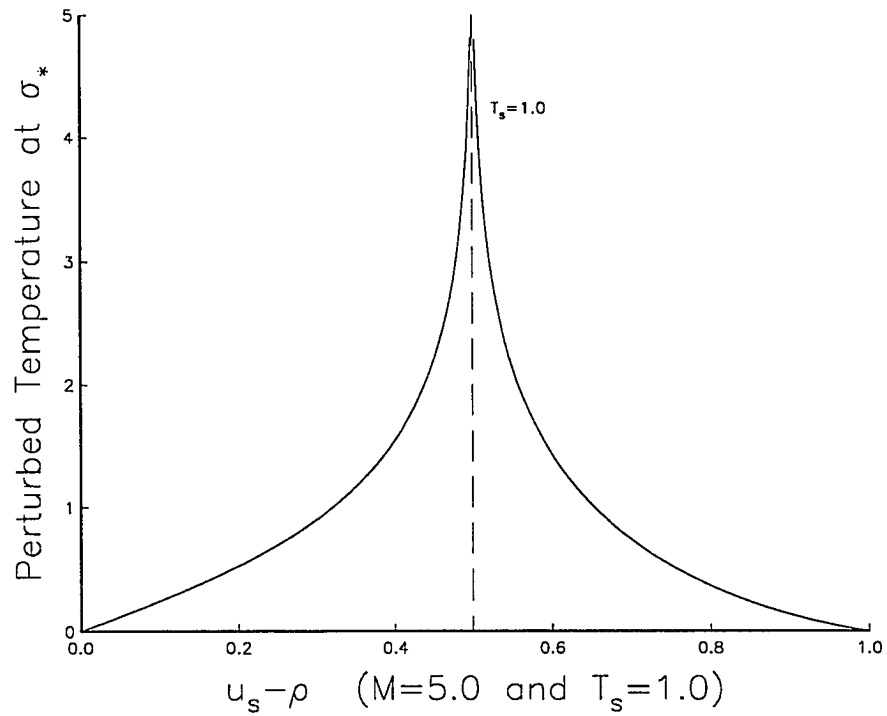
Figure 7.3: The perturbed temperature profile at $\sigma = \sigma_*$ as a function of $(u_s - \rho)$ for fixed Mach number $M = 5.0$ and surface temperature $T_s = 1$.

86

Figure 7.4: Ignition distance σ_* as a function of surface temperature T_s for fixed Mach number $M = 2.5$ and Prandtl number $P_r = 1$.

87

Figure 7.5: Ignition point $(u_s - \rho^*)$ as a function of surface temperature T_s for fixed Mach number $M = 2.5$.

Figure 7.6: Ignition distance σ_* as a function of Mach number M for fixed surface temperature $T_s = 1.0$ and Prandtl number $P_r = 1$.

Chapter 8

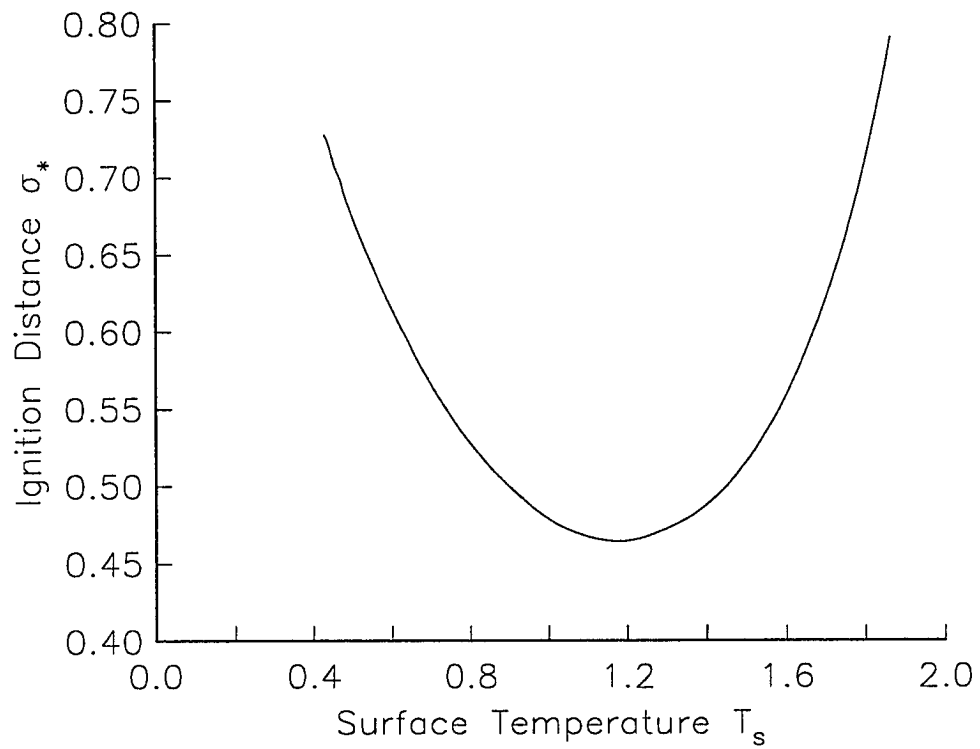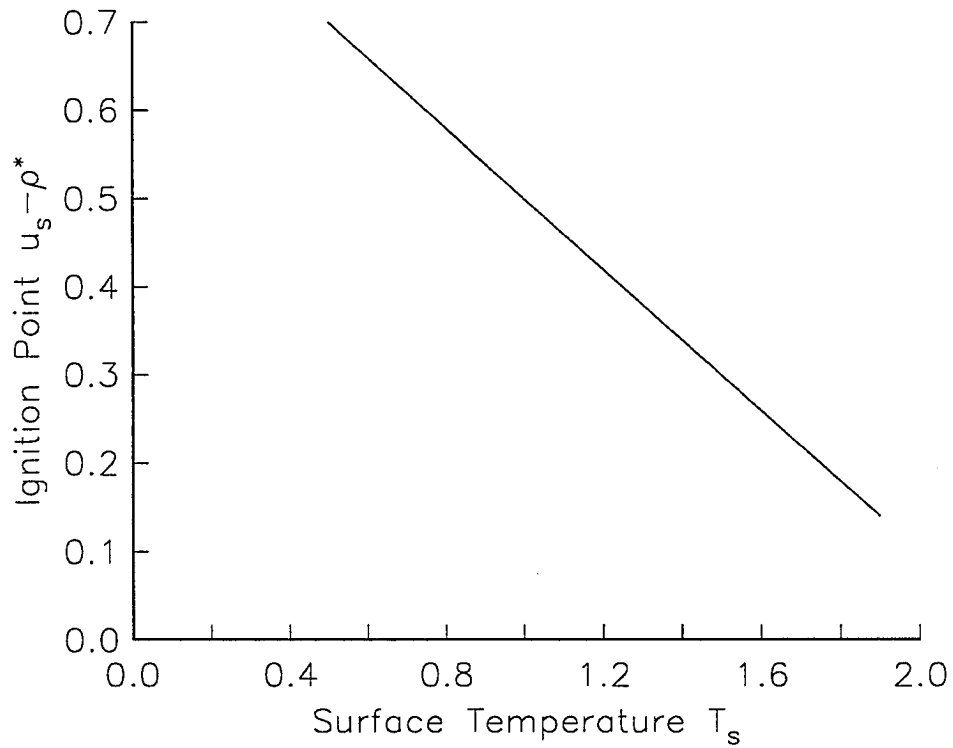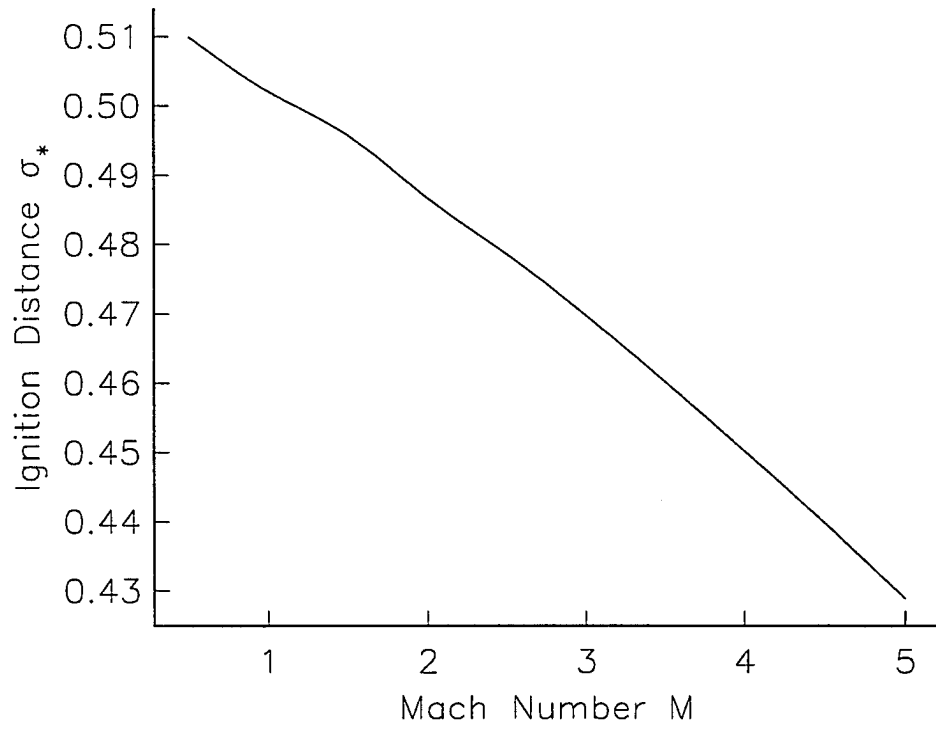# CONCLUDING REMARKS

Considered in the present study is the model of a planar shock front moving through a gas capable of undergoing an exothermic chemical reaction of the Arrhenius type. By including viscous terms and the presence of a wall, it is clear that a boundary layer develops behind the shock front. Asymptotic analysis in the limit of large activation energy is performed to investigate the ignition of this reactive gas in such a boundary layer. The analysis is done for both adiabatic boundary conditions with no transfer of heat across the wall and isothermal boundary conditions with the wall temperature held constant. Since thermal energy is created through viscous heating in the boundary layer, the ignition characteristics depend significantly on the magnitude and the form of the viscous heating term. Non-dimensionalization shows that the magnitude is proportional to the square of the Mach number, and using Sutherland's temperature-viscosity law provides a better approximation and more rapid variation of viscosity with respect to temperature than does the linear temperature-viscosity law. Im *et al.* [10] have studied a related problem using the linear temperature-viscosity law and not accounting for the effects of the shock. Their analysis and their

90

numerical calculations are simplified since the momentum and energy equations are uncoupled under these conditions. The use of the Sutherland's temperature-viscosity law presented here results in a coupling of the momentum and energy equations. The analysis and subsequent calculations are also considerably more involved. The effects of the shock are included and found to make significant differences in the inert temperature profile greatly affecting the ignition characteristics. A comparison is given for four cases: Sutherland's law with shock effects, Sutherland's law without shock effects, linear law with shock effects and linear law without shock effects. The cases with shock effects are referred to as the $u_s \neq 0$ cases, and the cases without shock effects are referred to as the $u_s = 0$ cases. Figure 3.2 shows that the magnitude of the second derivative of the adiabatic, inert-state temperature near the boundary using the Sutherland's law with shock effects is significantly larger than when using the linear law without shock effects. This is especially significant for large Mach numbers. The larger second derivative indicates the effects of viscous heating are more localized. The inert-state temperature profiles of Figure 3.3 and Figure 3.4 show also that, although the adiabatic wall-temperature is same for constant Mach number, changing from the $u_s = 0$ case to the $u_s \neq 0$ case localizes the viscous heating effects near the boundary. Interestingly, the velocity profiles in Figure 3.6 show no difference between the velocity profiles with $u_s = 0$ and with $u_s \neq 0$. Since it is the velocity profiles that govern the creation of thermal energy through viscous heating, it is determined at this point that the major differences in the two analyses occur in the convective terms only. The subsequent different balancing between convective and diffusive terms is observed in the temperature profiles in Figure 3.3 and Figure 3.4. The profiles differ in character for large distances from the wall, as well as for small distances, as previously noted. Temperature profiles for the isothermal boundary conditions in Figure 3.8 show that, although the maximum temperature is the same

91

for a constant Mach number and the surface temperature, changing from the $u_s = 0$ case to the $u_s \neq 0$ case localizes the viscous heating effects near the point of maximum temperature, but not as dramatically as in the adiabatic case. The same differences in the profiles appear for large distances from the wall.

The effects of the various parameters on the non-dimensional ignition distance and the ignition point are investigated for both the adiabatic and the isothermal boundary conditions. For the adiabatic boundary conditions, the non-dimensional ignition distance depends, mainly, on the Mach number M. It is found that the non-dimensional ignition distance σ_* decreases almost linearly with the Mach number as shown in Figure 5.3. In the isothermal wall case, there are two significant parameters, namely, the Mach number M and the surface temperature T_s. The effect of both parameters on the ignition distance and the ignition point is analyzed by keeping one of them constant and varying the other. The effects of the surface temperature on the ignition distance and the ignition point for the fixed Mach number are shown in Figure 7.4 and Figure 7.5 respectively. It is seen that with the fixed Mach number, the non-dimensional ignition point ρ^* decreases linearly with the surface temperature and the non-dimensional ignition distance σ_* decreases at first, and then starts to increase as the surface temperature increases. The extremes of these regions are characterized by the loss of a temperature maximum in the boundary layer. For decreasing T_s, the temperature maximum occurs further and further away from the wall, and for increasing T_s, the temperature maximum approaches the wall as the value of T_s approaches the value of the adiabatic wall-temperature for that Mach number. In both cases, the assumptions made to perform the asymptotic analysis contained here lose their validity.

It is concluded that the problem of ignition in the boundary layer behind a normal shock front is fundamentally different from the problem of supersonic flow past a flat

92

plate, as studied by Im *et al.* [10]. The analysis leads to identical velocity profiles (and, therefore, viscous heating) in terms of the proper similarity variables for each problem; however, the analysis shows that there are significant differences in the temperature profiles. Since the reaction term is temperature-sensitive, this leads to significant differences in the calculation of the ignition distance. However, it should be noted that the choice of T^*, which determines the exponentially varying length scales of the ignition problem, is the same for both cases. The differences in ignition distances are due mainly to the differences in curvature of the inert temperature profile at the ignition point. A change from the use of the linear-viscosity law to the more realistic Sutherland's viscosity law produces a similar change in the calculation of the ignition distance.

Bibliography

[1] Robert P. Benedict. *Fundamentals of Gas Dynamics.* John Wiley and Sons, pp. 30-33, 1983.

[2] John N. Bradley. *Shock Waves in Chemistry and Physics.* John Wiley and Sons, 1962.

[3] John D. Buckmaster. *The Mathematics of Combustion.* SIAM, 1985.

[4] S. I. Cheng and A. A. Kovitz. *Ignition in the Laminar Wake of a Flat Plate.* 6th Symp. (Intl.) Combust., Reinhold, p. 418, 1957.

[5] S. I. Cheng and A. A. Kovitz. Mixing and Chemical Reaction in the Laminar Wake of a Flat Plate. *J. Fluid Mech.,* Vol. 4, p. 64, 1958.

[6] J. F. Clarke and R. S. Cant. Nonsteady Gasdynamic Effects in the Induction Domain Behind a Strong Shock Wave. *Progress in Aeronautics and Astronautics,* 1984.

[7] D. A. Dooley. *Ignition in the Laminar Boundary Layer of a Heated Plate.* Heat Transfer and Fluid Mechanics Ins., Stanford University Press, pp. 321-42, 1957.

[8] Silva da Figueira, L. F., B. Deshaies and M. Champion. Numerical Study of Ignition Within Hydrogen-Air Supersonic Boundary Layers. *AIAA Journal*, Vol. 31, No. 5, 1993.

[9] C. E. Grosch and T. L. Jackson. Ignition and structure of a laminar diffusion flame in a compressible mixing layer with finite rate chemistry. *Phys. Fluids A*, Vol. 3, No. 12, pp. 3087-97, 1991.

[10] H. G. Im, J. K. Bechtold and C. K. Law. Analysis of Thermal Ignition in Supersonic Flat-Plate Boundary Layers. *J. Fluid Mechanics*, Vol. 249, pp. 99-120, 1993.

[11] T. L. Jackson and M. Y. Hussaini. An Asymptotic Analysis of Supersonic Reacting Mixing Layers. *Combust. Sci. Tech.*, Vol. 57, Nos. 4-6, pp. 129-40, 1988.

[12] T. L. Jackson and A. K. Kapila. Shock-Induced Thermal Runaway. *SIAM J. Appl. Math.*, Vol. 45, No. 1, 1985.

[13] Y. Ju, and T. Niioka. Ignition Analysis of Unpremixed Reactants With Chain Mechanism in a Supersonic Mixing Layer. *AIAA Journal*, Vol. 31, No. 5, pp. 863-68, 1993.

[14] C. K. Law and H. K. Law. Thermal Ignition Analysis in Boundary-Layer Flows. *J. Fluid Mechanics*, Vol. 92, p. 97, 1979.

[15] F. E. Marble and T. C. Adamson. Ignition and Combustion in a Laminar Mixing Zone. *Jet Propulsion*, Vol. 24, pp. 85-94, 1954.

[16] H. Schlichting. *Boundary Layer Theory.* 7th ed., McGraw-Hill, New York, 1979.

[17] O. P. Sharma and W. A. Sirignano. On the Ignition of a Premixed Fuel by a Hot Projectile. *Combust. Sci. Tech.,* Vol. 1, p. 481, 1970.

[18] C. Trevino and F. Mendez. Asymptotic Analysis of the Ignition of Hydrogen by a Hot Plate in a Boundary-Layer Flow. *Combust. Sci. Tech.,* Vol. 78, Nos. 4-6, pp. 197-216, 1991.

[19] F. A. Williams. *Combustion Theory.* 2nd Ed., Benjamin Cummings, 1985.

Appendix A

Derivation of the u_S versus M

Relation

The mean flow equations, which express conservation of mass-flux, normal momentum and enthalpy across a shock-like discontinuity, are

$$\rho_1' v_1' = \rho_2' v_2', \tag{A.1}$$

$$\frac{1}{2}v_1'^2 + \frac{a_1'^2}{\gamma - 1} = \frac{1}{2}v_2'^2 + \frac{c_2'^2}{\gamma - 1}, \tag{A.2}$$

and

$$p_1' + \rho_1' v_1'^2 = p_2' + \rho_2' v_2'^2 \tag{A.3}$$

where the subscripts 1 and 2 denote the regions ahead and behind the shock respectively. Also $v' = u' - u_s'$, where u' is the normal component of the velocity, u_s' is the speed of the shock wave and a' is the speed of sound.

97

These equations are non-dimensionalized by choosing the sound speed behind the shock wave as the characteristic velocity and by selecting ρ_1' and p_1' to be the units of density and pressure to get

$$\frac{\rho_1}{\rho_2} = \frac{\tilde{v}_2}{\tilde{v}_1}, \tag{A.4}$$

$$\frac{1}{2}\tilde{v}_1^2 + \frac{1}{\gamma - 1} = \frac{1}{2}\tilde{v}_2^2 + \frac{1}{\gamma - 1}\tilde{a}_2^2, \tag{A.5}$$

and

$$\frac{\rho_1}{\rho_2}[\frac{1}{\gamma} + \tilde{v}_1^2] = \frac{1}{\gamma}\tilde{a}_2^2 + \tilde{v}_2^2 \tag{A.6}$$

where $\tilde{v}_1 = v_1'/a_1'$, $\tilde{v}_2 = v_2'/a_1'$ and $\tilde{a}_2 = a_2'/a_1'$. Using equation (A.4) in equation (A.6) and simplifying gives

$$2\tilde{v}_1\tilde{a}_2^2 = 2(1 + \gamma\tilde{v}_1^2)\tilde{v}_2 - 2\gamma\tilde{v}_1\tilde{v}_2^2. \tag{A.7}$$

Similarly from equation (A.5),

$$2\tilde{v}_1\tilde{a}_2^2 = \tilde{v}_1(2 + (\gamma - 1)\tilde{v}_1^2) - \tilde{v}_1(\gamma - 1)\tilde{v}_2^2. \tag{A.8}$$

Subtracting equation (A.7) from equation (A.8) and simplifying gives

$$\tilde{v}_2 = \frac{(1 + \gamma\tilde{v}_1^2) \pm (1 - \tilde{v}_1^2)}{(\gamma + 1)\tilde{v}_1}. \tag{A.9}$$

Choosing the negative sign in the above equation gives $\tilde{v}_2 = \tilde{v}_1$. This physically means that there is no shock. Therefore, the positive sign is the proper choice, so choosing provides

$$\tilde{v}_2 = \frac{2 + (\gamma - 1)\tilde{v}_1^2}{(\gamma + 1)\tilde{v}_1}. \tag{A.10}$$

98

Solving equation (A.8) for $\tilde{a}_2^2$ gives

$$\tilde{a}_2^2 = 1 + \frac{1}{2}(\gamma - 1)(\tilde{v}_1^2 - \tilde{v}_2^2). \tag{A.11}$$

Now, define $M_1 = \tilde{v}_1$ and rewrite equation (A.10) as

$$\tilde{v}_2 = \frac{2 + (\gamma - 1)M_1^2}{(\gamma + 1)M_1}. \tag{A.12}$$

Using this in equation (A.11) and simplifying gives $\tilde{a}_2$ as

$$\tilde{a}_2^2 = \frac{4\gamma(\gamma - 1)M_1^4 - (2\gamma^2 - 12\gamma + 2)M_1^2 - 4(\gamma - 1)}{2(\gamma + 1)^2 M_1^2}. \tag{A.13}$$

By definition, the Mach number behind the shock is

$$M_2^2 = \frac{\tilde{v}_2^2}{\tilde{a}_2^2}. \tag{A.14}$$

Using equations (A.12) and (A.13) gives

$$M_2^2 = \frac{2 + (\gamma - 1)M_1^2}{2\gamma M_1^2 - (\gamma - 1)} \tag{A.15}$$

or

$$M_1^2 = \frac{2 + (\gamma - 1)M_2^2}{2\gamma M_2^2 - (\gamma - 1)}. \tag{A.16}$$

From equation (A.10)

$$\frac{v_1'}{v_2'} = \frac{(\gamma + 1)M_1^2}{2 + (\gamma - 1)M_1^2} \tag{A.17}$$

and using equation (A.16) in (A.17)

$$\frac{v_1'}{v_2'} = \frac{2 + (\gamma - 1)M_2^2}{(\gamma + 1)M_2^2}. \tag{A.18}$$

99

Now, from the definition of the original problem as seen schematically in figure (1.1b)

$$\frac{v_1'}{v_2'} = \frac{-u_s'}{u_\infty' - u_s'} \tag{A.19}$$

or

$$\frac{v_1'}{v_2'} = \frac{-u_s}{1 - u_s}. \tag{A.20}$$

Therefore, equation (A.17) is written as

$$\frac{-u_s}{1 - u_s} = \frac{2 + (\gamma - 1)M_2^2}{(\gamma + 1)M_2^2} \tag{A.21}$$

and solving for M_2 gives

$$M_2^2 = \frac{2(u_s - 1)}{2u_s + (\gamma + 1)}. \tag{A.22}$$

By definition

$$
\begin{aligned}
M_2 &= \frac{v_2'}{a_2'} \\
&= \frac{u_\infty' - u_s'}{a_2'} \\
&= M(1 - u_s).
\end{aligned}
\tag{A.23}
$$

Using this in equation (A.22) gives

$$M^2(1 - u_s^2) = \frac{2(u_s - 1)}{2u_s + (\gamma - 1)} \tag{A.24}$$

and solving for u_s produces the final result

$$u_s = \frac{(3 - \gamma)M + \sqrt{(\gamma + 1)^2 M^2 + 16}}{4M}. \tag{A.25}$$

100

Appendix B

Derivation of the Relations for ξ_t, ξ_x and $\xi_x u$

To derive the relations for ξ_t, ξ_x and $\xi_x u$, consider the following Howarth Dorodnitzyn variable transformation

$$\xi = \int_0^y \rho(x, y', t) dy', \tag{B.1}$$

$$\bar{x} = x, \tag{B.2}$$

and

$$\bar{t} = t \tag{B.3}$$

which gives the relations

$$\frac{\partial}{\partial x} = \frac{\partial}{\partial \bar{x}} + \xi_x \frac{\partial}{\partial \xi}, \tag{B.4}$$

$$\frac{\partial}{\partial y} = \rho \frac{\partial}{\partial \xi}, \tag{B.5}$$

101

and

$$\frac{\partial}{\partial t} = \xi_t \frac{\partial}{\partial \xi} + \frac{\partial}{\partial \bar{t}}. \tag{B.6}$$

Differentiating equation (B.1) with respect to t and using equation (B.6) for $\partial/\partial t$ on the right-hand side gives

$$\xi_t = \int_0^y (\xi_t \rho_\xi + \rho_{\bar{t}}) dy'. \tag{B.7}$$

Now, consider the transformation for the similarity variable η

$$\eta = \frac{\sqrt{u_s}\xi}{\sqrt{u_s t - \bar{x}}}, \tag{B.8}$$

$$X = u_s \bar{t} - \bar{x}, \tag{B.9}$$

and

$$\bar{\bar{t}} = \bar{t} \tag{B.10}$$

which gives

$$\frac{\partial}{\partial \xi} = \sqrt{\frac{u_s}{X}} \frac{\partial}{\partial \eta}, \tag{B.11}$$

$$\frac{\partial}{\partial \bar{x}} = \frac{\eta}{2X} \frac{\partial}{\partial \eta} - \frac{\partial}{\partial X}, \tag{B.12}$$

and

$$\frac{\partial}{\partial \bar{t}} = -\frac{u_s \eta}{2X} \frac{\partial}{\partial \eta} + u_s \frac{\partial}{\partial X} + \frac{\partial}{\partial \bar{\bar{t}}} \tag{B.13}$$

Using equations (B.11) and (B.13) in equation (B.7) gives

$$\xi_t = \int_0^y \{\xi_t \sqrt{\frac{u_s}{X}} \rho_\eta - \frac{u_s \eta}{2X} \rho_\eta + u_s \rho_X + \rho_{\bar{t}}\} dy'. \tag{B.14}$$

102

Now, from equation (B.1),

$$d\xi = \rho dy \tag{B.15}$$

and combining equations (B.8) and (B.9) gives

$$\eta = \sqrt{\frac{u_s}{X}}\xi. \tag{B.16}$$

Differentiating equation (B.16) and using relation (B.15) on the right-hand side provides the relation

$$d\eta = \sqrt{\frac{u_s}{X}}\rho dy. \tag{B.17}$$

The expression for ξ_t can be simplified as

$$\xi_t = \int_0^\eta \{\xi_t \frac{\rho'_\eta}{\rho} - \frac{1}{2}\sqrt{\frac{u_s}{X}}\eta' \frac{\rho_{\eta'}}{\rho} + u_s\sqrt{\frac{X}{u_s}}\frac{\rho_X}{\rho} + \sqrt{\frac{X}{u_s}}\frac{\rho_{\bar{t}}}{\rho}\}d\eta'. \tag{B.18}$$

Proceeding similarly, the expression for ξ_x is

$$\xi_x = \int_0^y \{\frac{1}{2}\frac{1}{\sqrt{u_s X}}\eta' \frac{\rho_{\eta'}}{\rho} - \sqrt{\frac{X}{u_s}}\frac{\rho_X}{\rho} + \xi_x \frac{\rho_{\eta'}}{\rho}\}d\eta'. \tag{B.19}$$

To derive the expression for $\xi_x u$, consider

$$\xi = \int_0^y \rho dy'. \tag{B.20}$$

Differentiating with respect to x gives

$$\xi_x = \int_0^y \rho_x dy' \tag{B.21}$$

103

and, therefore,

$$\frac{d}{dy}(\xi_x) = \rho_x.$$

(B.22)

Now, integrating by parts the integral $\int_0^y \xi_x u_{y'} dy'$ and using the relation (B.22) gives

$$\int_0^y \xi_x u_{y'} dy' = \xi_x u - \int_0^y \rho_x u dy'$$

(B.23)

which can be rearranged to get

$$\xi_x u = \int_0^y [\rho_x u + \xi_x u_{y'}] dy'.$$

(B.24)

Using equation (B.4) for ρ_x on the right-hand side provides

$$\xi_x u = \int_0^y [u\{\rho_{\bar{x}} + \xi_x \rho_\xi\} + \xi_x u_{y'}] dy'$$

(B.25)

and using equation (B.11) and (B.12) the above expression can be simplified to

$$\xi_x u = \int_0^\eta \{\frac{1}{2} \frac{u}{\sqrt{u_s X}} \eta' \frac{\rho_{\eta'}}{\rho} - u\sqrt{\frac{X}{u_s}} \frac{\rho_X}{\rho} + u\xi_x \frac{\rho_{\eta'}}{\rho} + \xi_x u_{\eta'}\} d\eta'.$$

(B.26)

104

Statement of Autobiography

The author was born January 1, 1956 in Naseera, Pakistan. He received a Bachelor of Science degree in Mathematics in 1976 and a Master of Science degree in Mathematics in 1978 from Punjab University, Lahore, Pakistan. He received a second Master of Science degree in Geophysics in 1982 from Quaid-i-Azam University, Islamabad, Pakistan and taught geophysics at Quaid-i-Azam University from 1982 to 1985.

The author migrated to the United States in 1985 and taught mathematics at Elizabeth City State University, Elizabeth City, North Carolina, from August 1985 to April 1986. From 1986 to the present, the author has taught mathematics at Norfolk State University in Norfolk, Virginia. He earned a Doctorate in Computational and Applied Mathematics from Old Dominion University in Norfolk, Virginia, in May 1995.